A COMPACT LABORATORY SETUP FOR ELECTRIC DRIVES EDUCATION

by

Shoaib Imtiyaz Shaikh

Submitted to the Graduate School of Engineering and Natural Sciences
in partial fulfillment of
the requirements for the degree of
Master of Science

Sabancı University

August 2016

A COMPACT LABORATORY SETUP FOR ELECTRIC DRIVES EDUCATION

APPROVED BY:

Asst. Prof. Dr. Meltem Elitaş
(Thesis Supervisor) .....

Prof. Dr. Mustafa Ünel .....

Asst. Prof. Dr Eray Baran .....

(Istanbul Bilgi University)

DATE OF APPROVAL: 10/08/2016

to my family

Acknowledgments

First and foremost, I would like to express my deepest gratitude to my supervisor Asst. Prof. Dr. Meltem Elitaş. I am grateful for her guidance, patience, motivation and kind advises. I would also like to thank Prof. Dr. Asif Şabanoviç for his patience and guidance during my thesis works.

I am thankful to my thesis jury, Prof. Dr. Mustafa Ünel and Asst. Prof. Dr. Eray Baran for accepting to be part of thesis jury and their valuable feedback.

I would like to thank Fiaz Ahmed and Akhtar Rasool for their invaluable support and motivation throughout the Master's program. Completion of this research would not have been possible without the valuable suggestions from Eray Baran and Burak Soner and therefore I would take this opportunity to thank them as well.

I would like to express my heart-felt gratitude to my family, they have been a constant source of love, support and strength all these years.

Lastly, I gratefully acknowledge the funding received from TÜBİTAK 2215 graduate scholarship programme.

A COMPACT LABORATORY SETUP FOR ELECTRIC DRIVES EDUCATION

Shoaib Imtiyaz Shaikh

ME, M.Sc. Thesis, 2016

Thesis Supervisor: Asst. Prof. Meltem Elitaş

Abstract

Electrical machines and electrical drives have a large number of applications in the industry such as automobile industry, energy equipments, robotics etc. These industries and research and development institutes, are in constant demand of qualified graduates who are trained in the respective fields. The academic institutes regularly update the curricula for training the graduates in line with these demands. Laboratory experiments, being an integral part of the curriculum, also needs regular updates. However, setting up and upgradation of a laboratory can be a difficult process due to financial and space constraints. Hence, development of a compact, low cost and easy to operate laboratory setup is always in demand.

Keeping in view the above needs, work has been carried in this thesis for the upgradation of an existing Mechatronics lab setup, Mechatro Lab. It is a compact and economical laboratory setup for the study of electrical machines. It is capable of demonstrating the working of various AC and DC motors. The setup, although good for performing basic open loop experiments, lacked closed loop control experiments. Moreover, the drive circuitry and the controller are obsolete. This setup, if upgraded, had the potential to be an excellent teaching aid for understanding the basics as well as control techniques of electrical machines. This thesis aims to replace the obsolete hardware components and add closed loop speed control experiments to the existing experiments. The closed loop speed control experiments have been implemented in computer software, hardware and their results are presented.

ELEKTRİKLİ TAHRİK SİSTEMLERİ EĞİTİMİ İÇİN KOMPAKT BİR DENEY SETİ

Shoaib Imtiyaz Shaikh

ME, Yüksek Lisans Tezi, 2016

Tez Danışmanlar: Yrd.Doç.Dr. Meltem Elitaş

Özet

Elektrik makinaları ve elektrikli tahrik sistemleri otomotiv, enerji ve robotik gibi birçok endüstriyel uygulama alanına sahiptir. Bu alanda çalışan sanayi ve araştırma kuruluşları saygın eğitime sahip nitelikli mezunlara ihtiyaç duyarlar. Akademik alanda çalışma yapan enstitüler bu ihtiyaca yönelik düzenli olarak müfredatlarının yenilenmesi eğiliminde olurlar. Laboratuvar ortamındaki deney setlerinin de niteliklerinin arttırılması gerekmektedir. Ancak, bu deney setlerinin yenilenmesi ve niteliklerinin arttırılması finansal ve fiziksel yerlerinin müsait olmaması gibi nedenlerle oldukça zor bir aşamadır. Bu sebeple ucuz ve kolay uygulanabilir deney seti oluşturmaya her zaman gereksinim duyulmuştur.

Yukarıda belirtilen ihtiyaçlar göz önüne alındığında, Mekatronik laboratuvarındaki mevcut deney setinin yenilenmesi bu tez çalışmasının konusu olmuştur. Bu deney seti elektrik makinaları için oldukça kompakt ve ekonomik bir set olup farklı birçok AC ve DC elektrik makinasını çalıştırabilir konumdadır. Mevcut durumda deney seti birçok açık çevrim kontrolü gerçekleştirebilir durumda olmasına rağmen, kapalı çevrim kontrol uygulamalarında eksikleri mevcuttu. Ayrıca sürücü elektronik devreleri oldukça eskiydi. Bu sebeple, mevcut deney setinin yenilenmesi elektrik makinaları ve kontrol tekniklerinin temellerinin anlaşılması için çok başarılı bir yardımcı eleman olacağı düşünülmektedir. Bu tez çalışması mevcut deney setindeki eski donanımların yenilenerek kapalı çevrim hız kontrolü deneylerinin de yapılabilir hale getirilmesini amaçlamıştır. Kapalı çevrim hız kontrolü deneyleri bilgisayar destekli yazılımlar yardımıyla yapılmıştır ve sonuçlar çalışmada gösterilmiştir.

Table of Contents

List of Figures

List of Tables

Chapter 1

Introduction

1.1 Introduction

Laboratory experiments play an important role in technical education and research. Generally, setting up experimental test benches is not feasible due to financial constraints, space requirements and technical expertise needed to operate them, especially in electrical engineering. One of the core areas of electrical and mechatronics engineering is the study of electrical machines and power electronics. Electrical machines are of various types based on the construction and the input power supply such as DC motor, synchronous motor, induction motor and stepper motor to name a few.

The combination of various electrical machines in one trainer setup with less space requirement and low cost is always in demand. One such product, The Mechatro Lab, was developed by Showa Dengyosha Co. Ltd. in the early 1990's. The Mechatro Lab is a compact mechatronics lab setup which can be used to demonstrate the operation of various motors. The setup consists of a drive circuitry, motor current and speed measurement devices and an assembly to build different motors. DC machines, AC machines (Synchronous and Asynchronous), Stepper motors are a few of the motors that could be assembled and experimented upon. The drive circuitry included a 3-phase inverter consisting of Power MOSFET's. These MOSFET's are driven by a PWM signal from a micro-controller.

Although this is a compact and economical setup, it is limited to test the motors in

open loop only. In other words, it lacks the closed loop control experiments of the motors. Additionally, the micro-controller used is based on the 8080, 8086 micro-processors which are no longer available in the market. The MOSFETs and other circuitry is also obsolete. In case any of these components malfunctioned, it would be difficult to find an exact replacement. Hence, the drive circuitry needed a complete overhaul. This trainer, if improved, can work as an excellent training module for understanding the basics as well as the implementation of various control techniques on electrical machines.

1.2 Literature Review

The study of electrical machines and power electronics is an integral part of electrical engineering. Due to its broad range of applications in the industry, it is mandatory that the students graduated with electrical engineering degrees should have understanding of them. This is possible if the students are trained in such a way that they have hands on experience while mastering the theoretical concepts. Since, these courses are difficult to understand if some practical experiments are not included in the course, laboratories are used as an aid to the classroom education. In [1], the authors were able to restructure the electric drives course by integrating power electronics, electric machinery and control in a single course. A DSP based laboratory was also built to be used in under-graduate as well as advanced level courses. Numerous approaches have been tried to develop and teach these courses so that students are trained to meet the needs of the industry and research institutions. These approaches include the traditional laboratories approach, computer based simulations and remote lab approach [2].

In the traditional laboratory approach, students perform experiments in small groups on existing setups available in a laboratory. In this approach, a commonly utilized method in the course and lab work is the building blocks method[3][4]. In this method the course topics are broken down into modules which are sequenced appropriately. Each module has its own set of experiments. This way the whole course content is covered in class leading to a better understanding.

The laboratory setup of power electronics and electric machinery requires the incorporation of gate driver circuits, supply isolation and controller circuitry. Making a working setup of these circuitry may take a considerable amount of time. This problem can be addressed by using a black box approach in which pre-built circuits can be interconnected to obtain a full working circuit in less time. A drawback of this approach is that if the inner circuit is not accessible it may lead to incomplete understanding of the experiments. An alternative to this approach is the blue box approach[5][6]. In this approach the pre-built circuitry is studied before they are implemented in the experiments. As the course progresses the students have a better understanding of these circuits and are equipped with the knowledge to build it themselves.

Project based learning in the laboratory is another approach which has been adopted [7–9]. In a traditional laboratory setting, students are expected to follow a set of instructions to perform an experiment. This way of teaching usually fails to create enthusiasm for learning. Whereas if the students were given real world projects based on the theory covered in the lectures, it would increase their motivation and enhance their learning [10]. A project may need knowledge of other related fields and it would motivate the students to learn about them and enhance their learning. L Goel, et al. in [11] suggested modifying the course content to be fully project based. In this approach, more emphasis is given on the practical implementation with the related theory being covered in class.

Some equipment in a physical lab may have a high cost, space constraints or safety concerns. In such a situation computer based simulations are the best solution. Simulations in electric machinery are helpful in understanding the dynamic behavior and analyzing its performance which may be unclear after reading the theory. It also provides us with the opportunity to test the machine response for unfavorable conditions without physically creating those conditions. This saves time and money and gives a glimpse of the machine response beforehand. Moreover, students can work using their own personal computers at a time and place convenient to them[12–14].

The computer programs such as MATLAB/Simulink, LabVIEW, Multisim, PSPICE are some of software's that have been integrated in the teaching methodology and are

widely used in the universities. In[15], the authors discuss the PSPICE and MATLAB/ Simulink applications in power electronics and electric drive system. As an example they implemented a DC−AC inverter circuit and a buck−boost converter using PSPICE and vector control of induction motor in Simulink. In [16], the authors recommend the utilization of Multisim to study and simulate power electronics circuits like power converters, frequency converters etc. They base their recommendation on the presence of numerous relevant libraries and built in data processing tools. In this thesis, MATLAB/Simulink is selected as the simulation tool due to its ease of availability and presence of relevant inbuilt libraries [15][17]. Although computer based simulations are advantageous, there are concerns about excessive reliance on them, which could lead to a disconnection between the real and simulated world. Moreover, simulations involve a simplification of the actual model, which needs to be considered while interpreting the results [14],[18–20].

A third approach that is being used in the power electronics and electrical machine labs is that of a remote laboratory[21]. The students are connected to the lab via the internet and can perform the experiments in real time. A camera is also used to display the real time status of the lab while performing the experiments. The students can change the parameters of the experiment, observe the results as well as download data. The students have access to the lab 24x7, unlike the traditional labs which are available at fixed times and physical presence is necessary. A number of experiments have been carried out in this regard[22][23]. In[24] the authors implemented experiments on a dc motor via remote access. The users can control the speed of the DC motor using a PID controller. They can vary the parameters, change the reference speed and store and download the speed response of a motor. Additionally experiments were also performed on coupled tanks[25], helicopter[26], ball and beam[27], dc-dc converter[21], inverted pendulum[28] to name a few.

Remote labs can be considered as an intermediary between the simulations approach and the traditional labs. This approach is favorable when lab space is limited or there is a requirement of distance learning. Distance learning is helpful for students belonging to institutes which do not have the required lab setup. Such institutes can collaborate

with a remote facility and provide the benefits of a regular lab to their students.

Taking into account the above three approaches, work has been carried out in this thesis to develop a compact lab setup for the study of electric drives by senior undergraduate and graduate electrical engineering students. It is a combination of the computer simulation and the traditional laboratories approach and can also be extended to accommodate the remote laboratory approach.

Finally, a short literature review of power converter is given here, without which the realization of modern applications may not be possible. Electric drives require a power converter between the source and the machine which connects and controls the power flow between the sources and the machine [29][30]. The type of power which operates the machine and the source may not be of the same type. In such a case power converters are used to perform the necessary conversions. As the converters are the link between the sources and the machines, they must be designed in such a way that they consume very little amount energy as possible[31]. The energy consumed by the converter reduces the efficiency of the conversion, hence they must be highly efficient. The use of modern control techniques especially sliding mode control has brought the converter technology much forward to be used in modern applications such as wind energy, motion control, robotics to name a few[32][33].

Chapter 2

System components and Thesis objectives

Laboratories generally need a large amount of space and are also in need of regular modernization, to keep pace with the demands of the industry. Establishment as well as modernization of laboratories also requires sufficient financial resources. Hence, the development of a compact, economical setup which can be used for performing basic as well as research oriented experiments will be an important addition for both, research and education. Due to these needs, a Mechatronics lab setup is developed for the study of electrical machines. Its components are discussed in this chapter.

2.1 Current Mechatro Lab Structure

The current Mechatro Lab setup consists of:

1. Power Supply unit (KENTAC-2202P-1): The power supply unit consists of two power supplies
   (a) DC 60V Power Supply 0-60V Approx, 0-4A Approx.
   (b) DC 18V Power Supply 0-18V Approx, 0-2A Approx.
2. Power converter unit and micro-controller: The DC - AC converter is standard 3 phase bridge interconnected to a Z8080 microcontroller board suitable for open

loop operation of different machines. The Z8080 board is not operational thus the converter cannot be used and speed control experiments of only DC machines can be operated.

3. Motor housing unit: It consists of stator and rotor assemblies as shown in Figure 2.1

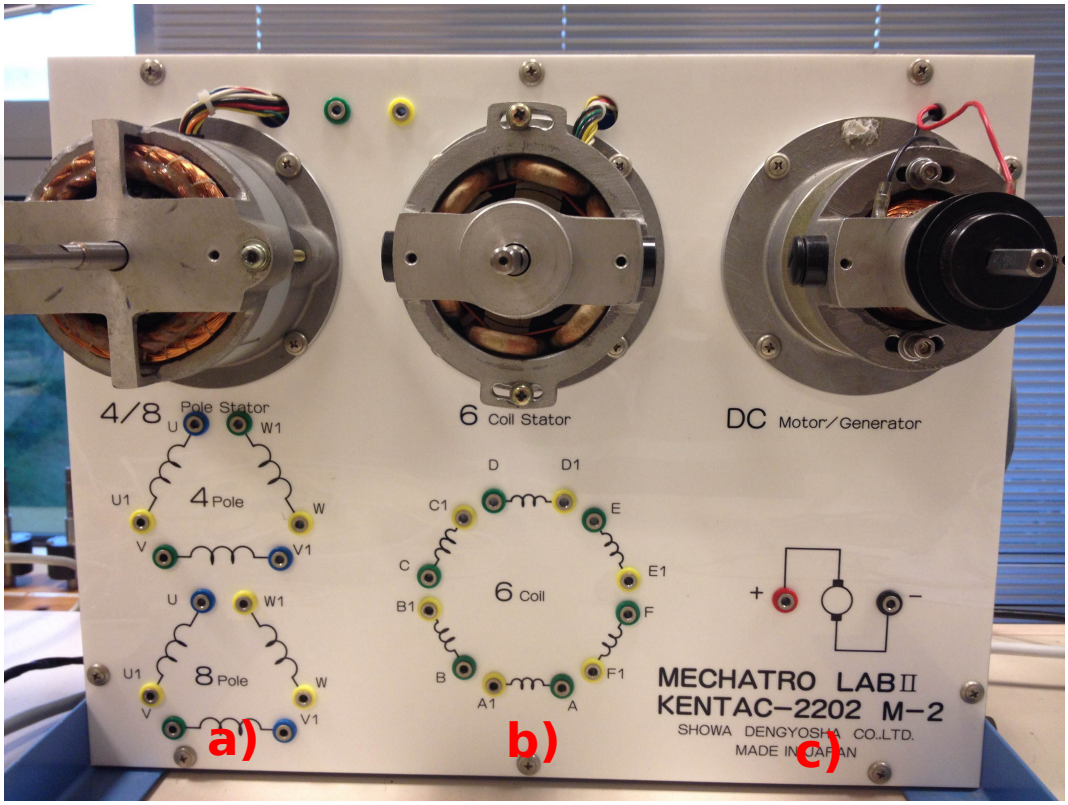

Figure 2.1: a) AC stator, b) 6-coil concentrated stator c) permanent magnet field stator

   (a) Stator assembly: It consists of 4,8 pole distributed winding stator, 6-coil concentrated winding stator and permanent magnet field stator

   (b) Rotor assembly: It consists of squirrel cage (copper and brass) rotor, reluctance rotor, hysteresis rotor, eddy current rotor, VR-type stepping rotor, 2 and 4 pole permanent magnet rotor and a commutator rotor.

AC stator: The AC stator has the option of having either 4 or 8 poles. The three phase terminals are available to connect them in either star or delta fashion.

6 coil concentrated stator: This stator can be used for the three phase stepper motor. Permanent magnet field stator: This stator is used for DC motor. The stator houses a ferrite type permanent magnet and has one pole pair. The rotor is fixed in the stator and should not be removed to maintain high efficiency.

2.2 Objective of the Thesis

The focus of this thesis is the up-grade of the Mechatronics trainer - Mechatro Lab. The main objective is to augment structure and equipment and allow application of the contemporary control techniques on electrical machines and in later stage on the power electronics converters.

The current structure should be augmented to allow extensive experimental work in closed loop electrical machines control. The overall structure of the desired laboratory structure can be described as in Figure 2.2.

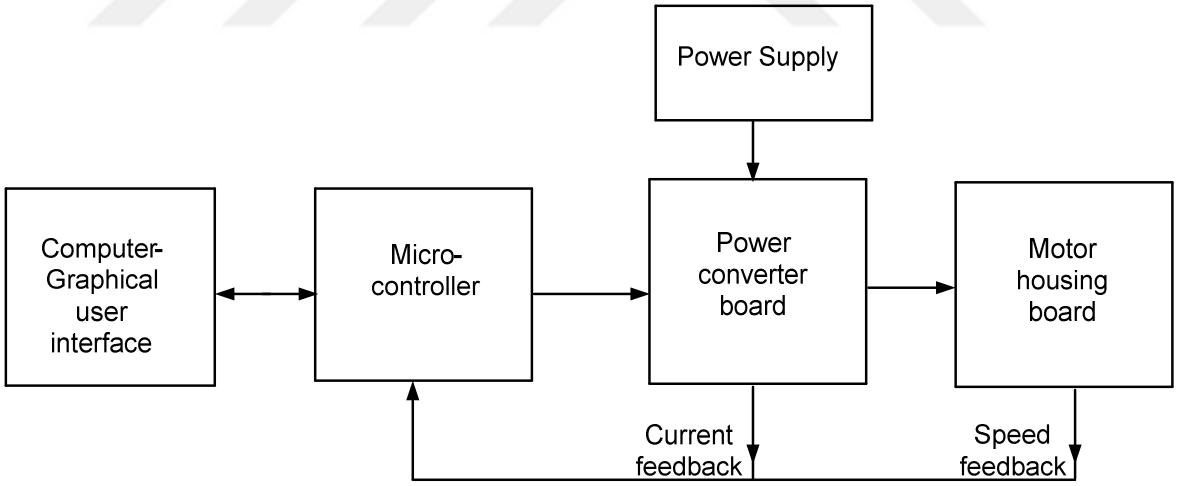

Figure 2.2: Overall structure of Mechatro Lab

1. Power converter board: Operated from the available sources up to 200V supply and able pass a highest current of 5A at room temperature. It also needs an optocoupler IC which isolates the micro-controller board from the high currents in the board.

2. Filter circuit: The LC filter circuit can be connected to the output of the power converter in different configurations allowing the experimentation with DC-to-DC and DC-to AC converters.

3. Measurement Unit: The setup also requires a current sensor and a rotary encoder to measure the current and speed/position respectively.

4. Control Unit: The control unit consists of the microcontroller board. The micro-controller board is needed for performing all the control operations on the motors by generating control signals for the power converter board.

5. Graphical user interface: A graphical user interface to enable users to observe and change certain variable data.

From the changes in the structure of the augmented Mechatrolab, follows the main objective of the thesis:

- Develop and implement necessary components and subsystems to augment the Mechatro Lab so that it can perform closed loop experiments on the electrical machines and later in development the power converters.

- Develop new power converter capable of supplying existing machines and suitable for further augmentation to include power electronics experiments in the setup.

- Incorporate affordable DSP based control equipment into the setup.

- Implement control of the DC and AC machines as an illustration of the system capability.

Chapter 3

Components and their Models

In this chapter the basic operation and the dynamic properties of the DC and AC machines are studied. The principle of energy conservation is applied to the electrical machine and a relation between the torque, current and angular displacement of the machine is derived. A general mathematical expression for electromagnetically coupled systems is also derived. The different type of converter topologies are also studied. The benefits of reference frame transformation are studied and also applied to the DC and AC machines.

3.1 Power Converters - Topology and operations

Power converter are used to connect two electrical energy sources and to control the power flow between them. Both sources can play a role of either electrical power generators or electrical power consumers [34].

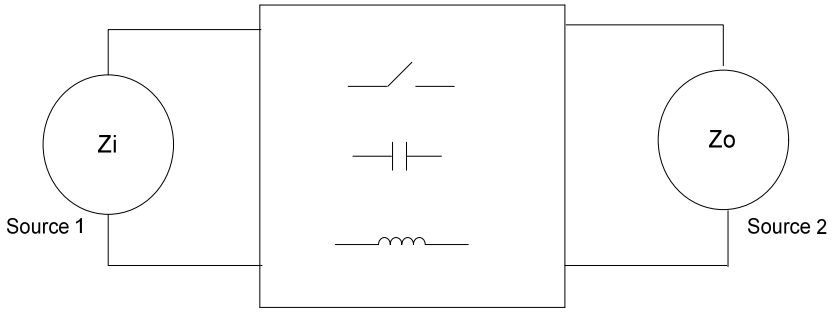

Figure 3.1: The connecting role of a switching converter

The power converter acts as a link between the power sources and power sinks. The state of an electric power source Z_i or electric power sink Z_o can be characterized by voltage u, current i and frequency f on its terminals $Z = (u, i, f)$. Not all three variables could be set independent for one source. The sources can be classified as either voltage or current sources. A voltage source, $Z_u = (u, f)$, can have independent voltage while its current is determined by the electric circuitry connected to its terminals. A current source, $Z_c = (i, f)$, has independent current while voltage across its terminals is determined by the electric circuitry connected to its terminals.

Consider a polyphase voltage source $Z_g = (u_g, f_g)$ and an electric power sink represented as a polyphase current source, $Z_s = (i_s, f_s)$. Transformation H acts upon the independent variables. Let the transformation H be defined by the matrix $\mathbf{M}$, so the relation between the sources and sinks can be written as:

$$\mathbf{u_s} = \mathbf{M}\mathbf{u_g} \tag{3.1}$$

where $\mathbf{u_g} = [u_{g1}\, u_{g2}\, \ldots\, u_{gn}]^T$, $\mathbf{u_s} = [u_{s1}\, u_{s2}\, \ldots\, u_{sn}]^T$.
The power generated by source and the power consumed by the load can be written as:

$$P_g = \mathbf{u_g}^T \mathbf{i_g} \tag{3.2}$$

$$P_s = \mathbf{u_s}^T \mathbf{i_s} = (\mathbf{M}\mathbf{u_g})^T \mathbf{i_s} = \mathbf{u_g}^T \mathbf{M}^T \mathbf{i_s} \tag{3.3}$$

where $\mathbf{i_g} = [i_{g1}\, i_{g2}\, \ldots\, i_{gn}]^T$, $\mathbf{i_s} = [i_{s1}\, i_{s2}\, \ldots\, i_{sn}]^T$.
From the assumption that the transformation is lossless and from equations 3.2 and 3.3

follows that the transformation acts upon independent variables of the load according to the following expression:

$$P_g = P_s \tag{3.4}$$

$$\mathbf{u_g}^T \mathbf{i_g} = \mathbf{u_g}^T \mathbf{M}^T \mathbf{i_s} \tag{3.5}$$

$$\mathbf{i_g} = \mathbf{M}^T \mathbf{i_s} \tag{3.6}$$

Transformation acts upon independent variables of both the source and the sink. The independent variables of the source and sink were arbitrarily selected, hence it implies that the role of source and sink can be interchanged.

3.1.1 Switching Matrix

Power converters should be designed in a way that they can connect any type of input and output sources together. The use of switches as a structural element of the converters offers the opportunity to consider a converter as the switching matrix as is shown in Figure 3.2.

Whenever a switch turns on, the corresponding input and outputs lines are connected. There are some conditions of the switches which cause a short circuit of the input voltages for a voltage source and an open circuit for a current source. Such conditions violate the Kirchoff's voltage and current laws and are considered as invalid.

Let us analyse the behavior of the switching matrix in Figure 3.2 with n input voltage sources, defined by the vector $\mathbf{u_g} = [u_{g1}\, u_{g2}\, \dots u_{gn}]^T$ and m current sinks, defined by the vector $\mathbf{i_o} = [i_{o1}\, i_{o2}\, \dots i_{om}]^T$. To satisfy the Kirchoff's laws only one switch which connects one of the n input lines to y-th ($y \in [1, ..., m]$) output line can be closed in any time interval. This requirement can be mathematically defined using the function $s_{xy}(t), x \in [1, 2, .., n]$, given by:

$$\sum_{x=1}^{n} s_{xy}(t) = 1, y \in [1, 2, ..m] \tag{3.7}$$

Equation 3.7 can be extended on the matrix $\mathbf{M}$ in the form:

$$\mathbf{Me} = \mathbf{e} \tag{3.8}$$

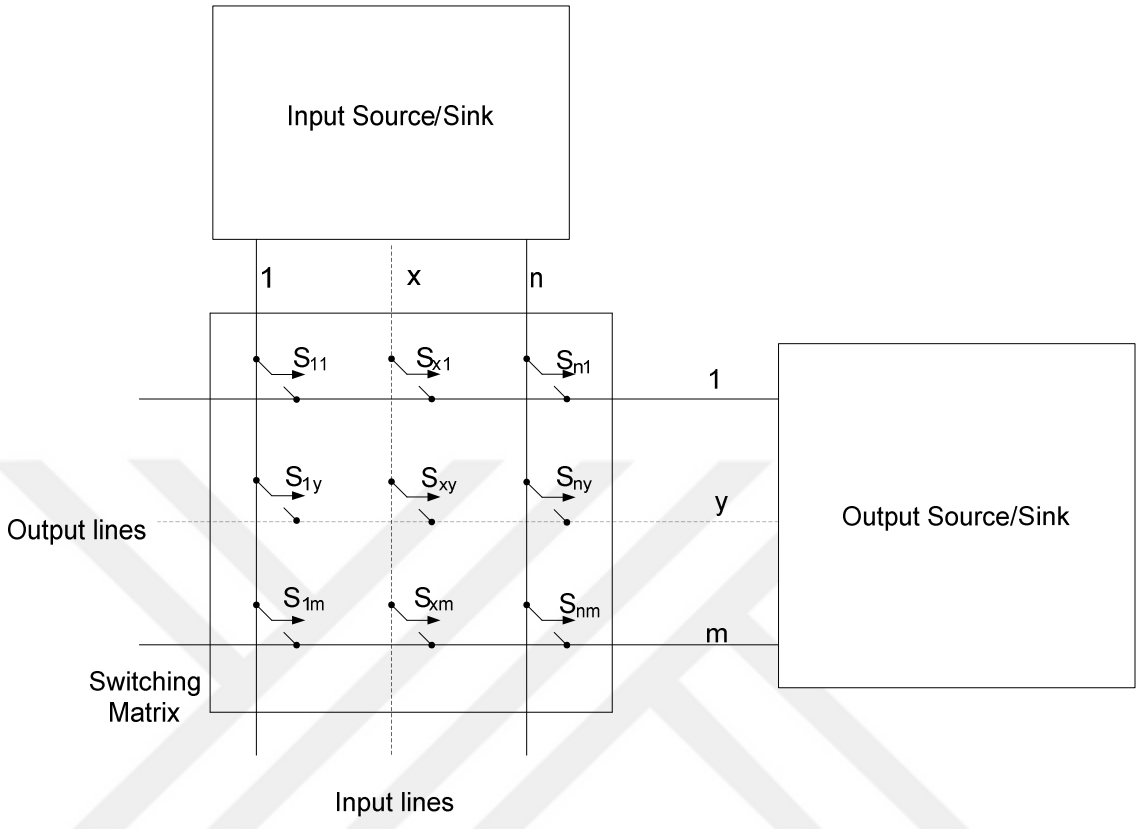

Figure 3.2: Structure of n-input m-output converter

where $\mathbf{e} = [1\,1\,\ldots 1]^T$.

Equation 3.7 implies that the switches are operated in a way that the short circuit of the voltage sources or open circuit of the current sources do not occur. Other implication is that the y-th output voltage can be calculated as:

$$u_{oy}(t) = \sum_{x=1}^{n} s_{xy} u_{gx} = s_y^T u_g \tag{3.9}$$

where $y \in [1, 2, ..m]$ and $\mathbf{s_y} = [s_{1y}\, s_{2y}\, \ldots\, s_{ny}]^T$. The output voltage is a weighted sum of the inputs. Combining all m outputs into one output vector
$\mathbf{u_o} = [u_{o1}\, u_{o2}\, \ldots\, u_{om}]^T$ the equation 3.9 can be rewritten as:

$$\mathbf{u_o(t)} = \mathbf{M(t)u_g(t)} \tag{3.10}$$

Elements of the matrix $\mathbf{M(t)}$ are the switching functions $s_{xy}(t)$, which define the states of switches in the switching matrix:

$s_{xy}(t) = 1$ with switch S_{xy} ON

$s_{xy}(t) = 0$ with switch S_{xy} OFF

The transformation of the currents, defined by the sinks connected to the output lines can be determined in the same way. The sinks being independent current sources cannot be left in open circuit, so constraints of equation 3.7 are applicable here as well. The current in the x-th input line is given by:

$$i_{gx}(t) = \sum_{y=1}^{m} s_{xy} i_{oy} = s_x^T i_o \tag{3.11}$$

where $x \in [1, 2, ..n]$

This expression can be combined in matrix equation:

$$\mathbf{i_g(t)} = \mathbf{M(t)}^T \mathbf{i_o(t)} \tag{3.12}$$

where $\mathbf{M(t)}^T$ is the transposed matrix $\mathbf{M}$. This result is in agreement with equation 3.4-3.6 obtained for general transformation.

We can now calculate the output voltages and input currents using the input voltages, output currents and the switching method of the switches.

The selection of the switching method or switching function $s_{xy}(t)$ is the calculation of the time duration for which switch $S_{xy}(t)$ is ON ($s_{xy}(t) = 1$) or OFF ($s_{xy}(t) = 0$). The switching period T is defined as the time period between two consecutive switching ON's. If T is short in comparison with frequency of sources and sinks then the time duration for which the switch $S_{xy}(t)$ is switched ON ($\frac{t_{ONxy}}{T} = \mu_{xy}$), is equal to the average value of the function $s_{xy}(t)$ over the period T:

$$\mu_{xy}(t) = \frac{1}{T} \int_t^{t+T} \frac{t_{ON} s_{ON} - t_{OFF} s_{OFF}}{T} dt \tag{3.13}$$

If $\bar{\mathbf{M}}$ is the matrix consisting of elements $\mu_{xy}(t)$, then the converter's operation can be described as:

$$\mathbf{u_o(t)} = \bar{\mathbf{M}} \mathbf{u_g} \tag{3.14}$$

$$\mathbf{i_g(t)} = \bar{\mathbf{M}}^T \mathbf{i_o} \tag{3.15}$$

$$\bar{\mathbf{M}} \mathbf{e} = \mathbf{e} \tag{3.16}$$

3.1.2 The interaction between sources and switches

A power converter is defined as a device for interconnecting two sources. To obtain control over the power flow, switches must be able to control their turn-ON and turn-OFF time, or both. In this section we will assume that switches are ideal and they can control both: turn-ON and turn-OFF time without restriction on the time intervals being switched ON or OFF. The switch can be regarded as ideal short circuit when they are ON and ideal open circuit when they are OFF.

Voltage Source Converters

The basic structure of a converter with a voltage source at input and a current source on output could be represented as in Figure 3.3. The switching matrix in Figure 3.3 consists of two switches connected in series.

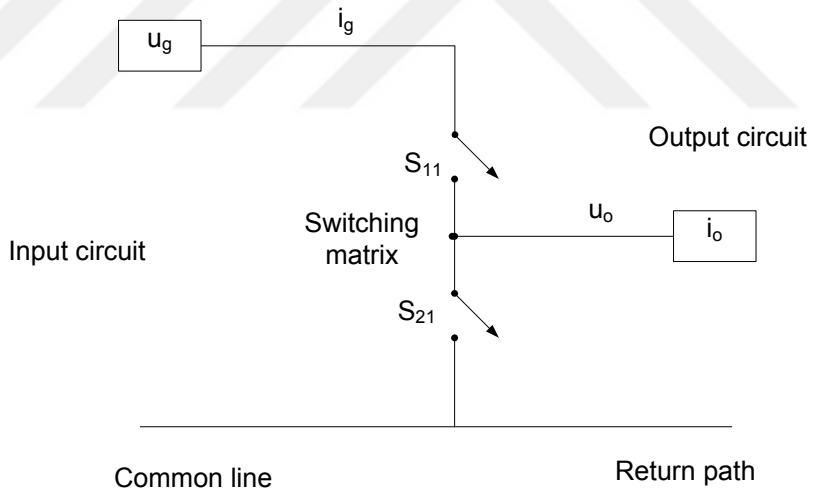

Figure 3.3: Structure of single input single output converter

The operation of the structure is described by the following equations:

$$u_o = u_g \tag{3.17}$$

$$i_g = i_o \tag{3.18}$$

for $S_{11} = ON$ and $S_{21} = OFF$

$$u_o = 0 \tag{3.19}$$

$$i_g = 0 \tag{3.20}$$

for $S_{11} = OFF$ and $S_{21} = ON$.

Selecting variable $s(t)$ such that it has value $s(t) = 1$ for $S_{11} = ON$ and $S_{21} = OFF$ and $s(t) = 0$ for $S_{11} = OFF$ and $S_{21} = ON$, the dependent variables on the output u_o and on the input i_g can be derived as:

$$u_o = u_g s \tag{3.21}$$

$$i_g = i_o s \tag{3.22}$$

The variable $s(t)$, is the control, as it defines the connection of the switches in the converter. Replacing the discontinuous function $s(t)$ with its average value $\mu \in [0, 1]$ as shown in equation 3.13, the range of change of the dependent variables can be calculated as:

$$0 \leq u_o \leq u_g \tag{3.23}$$

$$0 \leq i_g \leq i_o \tag{3.24}$$

This structure is known as the DC-to-DC buck converter.

The structure of the switching matrix in converters with one input and two output lines is illustrated in Figure 3.4 The output voltage can have three different values depending

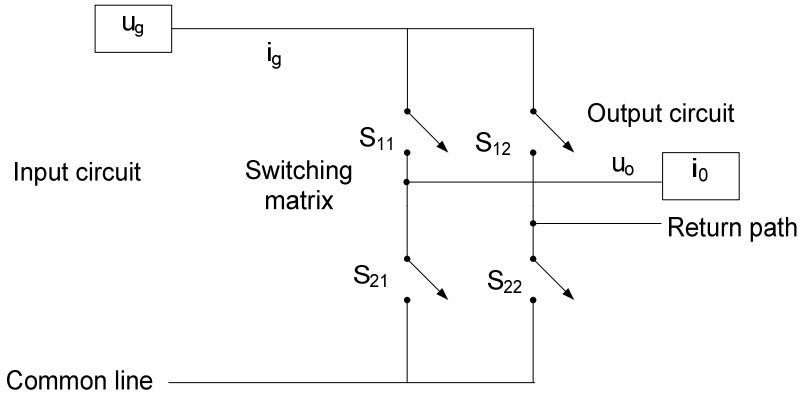

Figure 3.4: Structure of single input two output converter

on the state of the switches S_{11} to S_{22}:

$u_o = u_g$ with S_{11} and S_{22} switched ON;

$u_o = 0$ with S_{11} and S_{12} or S_{21} and S_{22} switched ON;

$u_o = -u_g$ with S_{12} and S_{21} switched ON;

The switches S_{11} and S_{21} or S_{12} and S_{22}, cannot be switched ON or OFF simultaneously.

The operation of the voltage source converter can be described as:

$s_x(t) = 1$ with switch S_{1x} ON and S_{2x} OFF

$s_x(t) = 0$ with switch S_{1x} OFF and S_{2x} ON

$x = 1, 2.$

$$u_o = u_g s_1 - u_g s_2 = u_g(s_1 - s_2) \tag{3.25}$$

$$i_g = i_o s_1 - i_o s_2 = i_o(s_1 - s_2) \tag{3.26}$$

By selecting $s = s_1 - s_2$ these equations can be rewritten as:

$$u_o = u_g(s_1 - s_2) = u_g s \tag{3.27}$$

$$i_g = i_o(s_1 - s_2) = i_o s \tag{3.28}$$

$s \in [-1, 0, 1]$.

The structure of the switching converters with three output lines is represented in Figure 3.5. The components of the control are defined as: $s_x(t) = 1$ with switch S_{1x} ON and

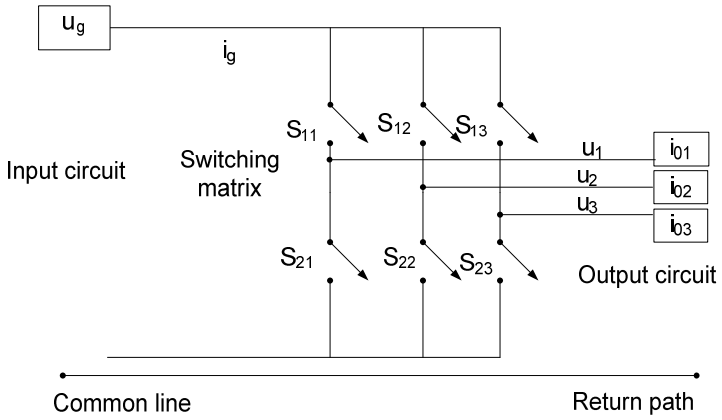

Figure 3.5: Structure of single input three output converter

S_{2x} OFF

$s_x(t) = 0$ with switch S_{1x} OFF and S_{2x} ON

$x \in [1, 2, 3]$.

The voltages on the output lines of the switching matrix and currents in input lines of the switching matrix can be expressed in the form:

$$\mathbf{u_x} = u_g \mathbf{s_x} \Rightarrow \mathbf{u} = u_g \mathbf{s} \tag{3.29}$$

$$i_g = i_{o1}s_1 + i_{o2}s_2 + i_{o3}s_3 \Rightarrow \mathbf{i_g} = \mathbf{i_o}^T \mathbf{s} \tag{3.30}$$

where $\mathbf{u} = [u_1 u_2 u_3]^T$ switching matrix output voltage vector,

$\mathbf{i_o} = [i_{o1} i_{o2} i_{o3}]^T$ load sources current vector,

$\mathbf{s} = [s_1 s_2 s_3]^T$ control vector,

u_g, i_g input voltage and current respectively.

The actual arrangement of the load should be taken into account to calculate the voltages on every phase of the loads. In the case of a symmetrical load, the voltages in star connection (Figure 3.6) can be expressed in the form:

$$\begin{bmatrix} u_{o1} \\ u_{o2} \\ u_{o3} \end{bmatrix} = \frac{1}{3} \begin{bmatrix} 2 & -1 & -1 \\ -1 & 2 & -1 \\ -1 & -1 & 2 \end{bmatrix} \begin{bmatrix} u_1 \\ u_2 \\ u_3 \end{bmatrix} = \frac{1}{3} \mathbf{A_Y u} = \frac{1}{3} \mathbf{A_Y} u_g \mathbf{s} \tag{3.31}$$

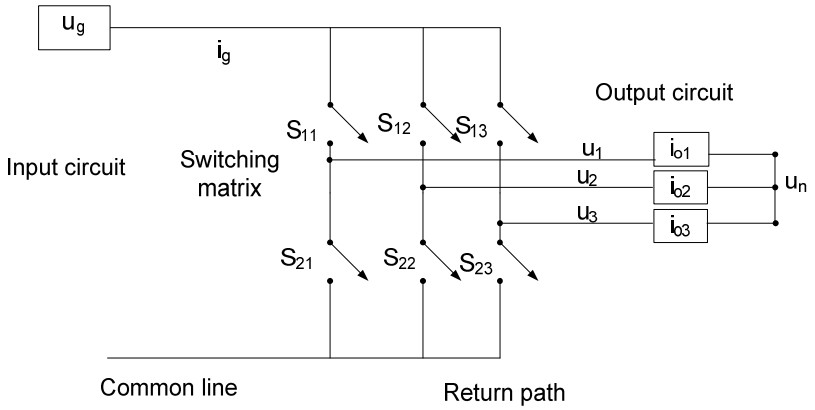

Figure 3.6: Converter with star connection on the load side

If a load is connected in delta connection (Figure 3.7) then phase voltages are defined by the relation:

$$\begin{bmatrix} u_{o12} \\ u_{o23} \\ u_{o31} \end{bmatrix} = \begin{bmatrix} 1 & -1 & 0 \\ 0 & 1 & -1 \\ -1 & 0 & 1 \end{bmatrix} \begin{bmatrix} u_1 \\ u_2 \\ u_3 \end{bmatrix} = \mathbf{A_\Delta u} = \mathbf{A_\Delta} u_g \mathbf{s} \tag{3.32}$$

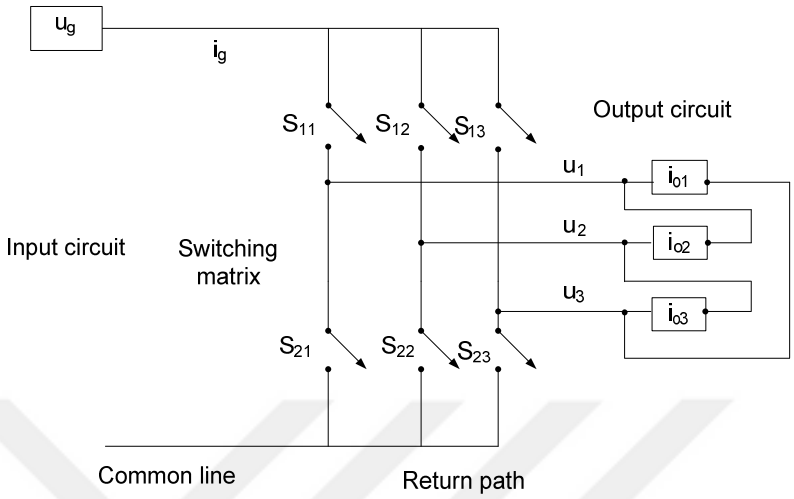

Figure 3.7: Converter with delta connection on the load side

This converter can also be used as a three phase symmetrical source by projecting the obtained load voltages into the frame of reference of the three phase symmetrical system. Let the voltages on a load form a three-phase group u_a, u_b, u_c with the basis vectors e_a, e_b, e_c. In general case when voltages u_a, u_b, u_c are not symetric $u_a+u_b+u_c = u_N \neq 0$. If phase voltages are symmetric then $u_a + u_b + u_c = u_N = 0$.

Let basis vectors e_A, e_B, e_C in an orthogonal frame of references (α, β) be shifted from each other for $\frac{2\pi}{3}$. Then:

$$e_a = [1, 0]^T \tag{3.33}$$

$$e_b = [-\frac{1}{2}, \frac{\sqrt{3}}{2}]^T \tag{3.34}$$

$$e_c = [-\frac{1}{2}, -\frac{\sqrt{3}}{2}]^T \tag{3.35}$$

Let the load phase voltages u_{o1}, u_{o2}, u_{o3} satisfy conditions to form symetric three phase source with phase voltages denoted as: $u_{o1} = u_a = Ucos(wt)$, $u_{o2} = u_b = Ucos(wt+\frac{2\pi}{3})$, $u_{o3} = u_c = Ucos(wt + \frac{4\pi}{3})$. It is convenient to make further analysis by projecting original voltages into new frame of references with two orthogonal axes α and β. The third component will represent the sum of the phase voltages. New frame of references

will be denoted as $(\alpha, \beta, 0)$. This transformation can be written as:

$$\mathbf{u}_{\alpha\beta 0} = (\mathbf{A}_{\alpha,\beta}^{a,b,c})^T \mathbf{u}_{abc} \tag{3.36}$$

$$\mathbf{u}_{\alpha\beta 0}^T = [u_\alpha u_\beta u_0] \tag{3.37}$$

$$\mathbf{u}_{abc}^T = [u_a u_b u_c] \tag{3.38}$$

In this case transformation matrix should be selected to satisfy conditions $(\mathbf{A}_{\alpha,\beta}^{a,b,c})^T \mathbf{A}_{\alpha,\beta}^{a,b,c} = \mathbf{E}$; $\mathbf{E}$ is is unity matrix. To satisfy given requirements the transformation matrix $\mathbf{A}$ should be selected in the form:

$$(\mathbf{A}_{\alpha,\beta}^{a,b,c})^T = \sqrt{\frac{2}{3}} \begin{bmatrix} \mathbf{A}_{\alpha,\beta} \\ \mathbf{b}^T \end{bmatrix} \begin{bmatrix} e_a & e_b & e_c \\ b_a & b_b & b_c \end{bmatrix} \tag{3.39}$$

$$\mathbf{A}_{\alpha,\beta} = \begin{bmatrix} e_{a\alpha} & e_{b\alpha} & e_{c\alpha} \\ e_{a\beta} & e_{b\beta} & e_{c\beta} \end{bmatrix} = \begin{bmatrix} 1 & -\frac{1}{2}, & -\frac{1}{2} \\ 0 & \frac{\sqrt{3}}{2} & -\frac{\sqrt{3}}{2} \end{bmatrix} \tag{3.40}$$

$$\mathbf{b}^T = [b_a b_b b_c] = [\frac{\sqrt{2}}{2} \frac{\sqrt{2}}{2} \frac{\sqrt{2}}{2}] \tag{3.41}$$

Taking into account expression that relates the switch control variables u_i 3.29-3.30 the switching matrix output variables and load phase voltages, equations 3.31 or 3.32 , the transformations equations 3.36 - 3.39 could be calculated for different load connections in the following form:

$$\mathbf{u}_{\alpha\beta 0} = (\mathbf{A}_{\alpha,\beta}^{a,b,c})^T \mathbf{A}_{\mathbf{Y\Delta}} s \tag{3.42}$$

$\mathbf{A}_{\mathbf{Y\Delta}} = \mathbf{A}_{\mathbf{Y}} or \mathbf{A}_{\mathbf{\Delta}}$

For symmetrical load in star connection the transformation equation 3.42 when applied to the 3.42 has the form:

$$\mathbf{u}_{\alpha\beta 0} = u_g \sqrt{\frac{2}{3}} \begin{bmatrix} 1 & -\frac{1}{2}, & -\frac{1}{2} \\ 0 & \frac{\sqrt{3}}{2} & -\frac{\sqrt{3}}{2} \\ 0 & 0 & 0 \end{bmatrix} \begin{bmatrix} s_1 & s_2 & s_3 \end{bmatrix} \tag{3.43}$$

where s_1, s_2, s_3 stand for the control of the switches in converter phases, and are defined as in 3.29. The component u_N is proportional to the sum of control vector components and is omitted from the analysis on the ground that average value of the phase voltages

form a balanced set defined by $u_a + u_b + u_c = u_N = 0$, and consequently the average values of the control vector components must satisfy the same restriction.
For the expression 3.43 averaging technique that was applied for DC-to-DC converters can be applied. The discontinuous control $s_x(x = 1, 2, 3)$ will be replaced by its average value μ_x. The range of the phase voltages, for selected average values of the control μ_x can be easily calculated. On the other hand, if $(u_\alpha u_\beta u_0)$ is given, then $(s_1 s_2 s_3)$ can also be determined as the transformation 3.43 is regular [35–37].

3.2 Energy conversion principle

Energy exists in various forms in nature such as heat, tidal, wave etc and can be converted from one form to another form of energy. In electric machines, energy conversion is between the electrical and mechanical energies. The electrical and mechanical energies are related to the electrical and mechanical sub systems respectively. The study of electric machines can be separated into electrical sub-system, mechanical sub-system and a coupling system. The electrical and mechanical sub-system is connected to external world by the electrical and mechanical terminals respectively. These terminals can act either as a source or a sink. The mechanical motion is a result of the interaction of the electrical and mechanical energies via the coupling system. The coupling system consists of the storing components from the electrical and mechanical sub-systems. The energy transfer from either of the sub-systems is done via the coupling components and this transfer is governed by the law of conservation of energy. According to law of energy conservation, the supplied energy should always balance the output energy plus losses. If the energy conservation principle is applied to an electrical machine, it can be stated as follows;

$$W_e + W_m = W_f + W_l \tag{3.44}$$

Where W_e, W_m are the input electrical and mechanical energies, W_l is the energy dissipated due heat loss in the electrical and the mechanical sub-systems and W_f is the energy stored in the coupling system. If energy is supplied by the source then it is assigned a positive sign and if energy is supplied to the source then it is assigned a

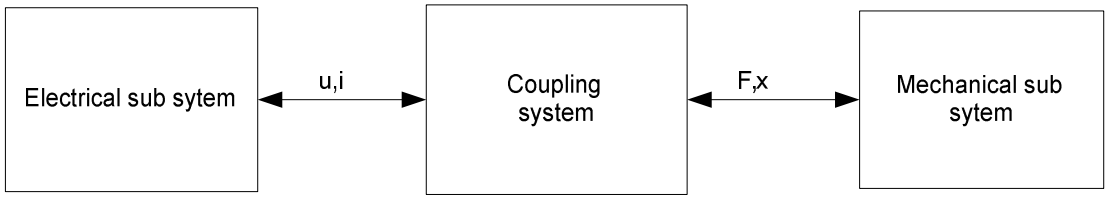

Figure 3.8: An electromechanical system

negative sign. If the losses are ignored, the energy balance for an electrical machine with single electrical input and single mechanical output can be written as;

$$dW_e(t) + dW_m(t) = dW_f(t) \tag{3.45}$$

$$P_e(t)dt + P_m(t)dt = dW_f(t) \tag{3.46}$$

where $dW_e(t)$, $dW_m(t)$ are the differential input electrical and mechanical energy and $dW_f(t)$ storing energy; $P_e(t)$ and $P_m(t)$ are electrical and mechanical power respectively. Let u,i be the input voltage and current flowing through the electrical sub-system, f and v the force and the velocity on the mechanical sub-system, then above expressions can be rewritten as:

$$u(t)i(t)dt + f(t)v(t)dt = dW_f(t) \tag{3.47}$$

$$u(t)i(t)dt + f(t)dx = dW_f(t) \tag{3.48}$$

Here dx is the displacement during the time increment dt. The mechanical force $f(t)$ is generated due to the input electrical energy, and is assigned a negative sign, as per the adopted sign convention. The above equation can be re-arranged as

$$u(t)i(t)dt - dW_f(t) = f(t)dx \tag{3.49}$$

Using Faradays law, flux can be represented with voltage u as follows

$$\frac{d\lambda}{dt} = u(t) \tag{3.50}$$

Now, the equation 3.49 can be re-written as

$$d\lambda(t)i(t) - dW_f(t) = f(t)dx \tag{3.51}$$

The displacement variable dx completely describes the mechanical system whereas for the electromechanical system flux $d\lambda(t)$ or current $i(t)$ can be used. If current and displacement are chosen as the independent variable, the total differential stored energy and the flux linkage can be written as

$$dW_f(t) = \frac{\partial dW_f(x,i)}{\partial x}dx + \frac{\partial dW_f(x,i)}{\partial i}di \tag{3.52}$$

$$d\lambda = \frac{\partial \lambda(x,i)}{\partial x}dx + \frac{\partial \lambda(x,i)}{\partial i}di \tag{3.53}$$

Substituting equation 3.52 and equation 3.53 in equation 3.49, we get,

$$f(t)dx = id\lambda(t) - dW_f(t) = (i\frac{\partial \lambda(x,i)}{\partial x} - \frac{\partial dW_f(x,i)}{\partial x})dx + (i\frac{\partial \lambda(x,i)}{\partial i} - \frac{\partial dW_f(x,i)}{\partial i})di \tag{3.54}$$

$\frac{\partial \lambda(x,i)}{\partial i}$ can be calculated from the stored energy equation $W_f(i,\lambda) = \int(i, d\lambda) = id\lambda - \int \lambda di$. Therefore,

$$f(t)dx = (i\frac{\partial \lambda(x,i)}{\partial x} - \frac{\partial dW_f(x,i)}{\partial x})dx \tag{3.55}$$

Using the relation

$$W_f(t) + W_{fd}(t) = i\lambda \tag{3.56}$$

where $W_{fd}(t)$ is the magnetic co-energy, the force can be written as $f(t) = \frac{\partial W_{fd}(x,i)}{\partial x}$. The electromagnetic system is electrically linear if the flux is linearly dependent on the current, thus $\lambda(t) = L(x)i(t)$ where $L(x)$ is single valued scalar function of the displacement. The magnetic energy can be written as $W_f(t) = \frac{L(x)i(t)}{2}$ or in vector case $W_f(t) = \frac{i(t)^T L(x) i(t)}{2}$, and it is equal to the magnetic co-energy. Then mechanical force becomes:

$$f(t) = \frac{\partial L}{2\partial x}i^2 = \frac{\partial i}{2\partial x}\lambda \tag{3.57}$$

From the above equation it can be seen that the mechanical force depends on flux and rate of change of current.

3.3 Dynamics of Electric machines

The dynamic equations of motion for an electric machine can be derived from the Faraday's law and Kirchhoff's law for electrical subsystem and d'Alambert's principle

for the mechanical subsystem. The electrical sub-system consists of only sources and resistive components. The resistor is connected in series with the source and the coupling system. The mechanical sub-system consists of a single cylinder structure which can rotate about its axis. The rotating motion is a result of the torque generated due to the interaction of the electrical and mechanical sub-systems.

Consider an electrical machine with an input u, resistance R and flux linkage λ acting as the coupling link, the electrical sub-system can be written as

$$\frac{d\lambda(t)}{dt} + Ri = u \tag{3.58}$$

where $\frac{d\lambda(t)}{dt}$ is induced electromotive force at the electric terminal.
The mechanical sub-system behavoir can be written as

$$\frac{d\theta(t)}{dt} = w \tag{3.59}$$

$$\frac{d(Jw)}{dt} = T_e - T_L \tag{3.60}$$

where θ is the angular position, w is the angular velocity, J is a moment of inertia of the rotor, T_e is the generated torque and T_L is load torque.
The equations 3.58-3.60 described the behavior of a single electrical input and a single mechanical output. Electrical machines have a single mechanical output but can have more than one electrical input. Next we will derive general equations for a machine with n electrical inputs.
An electrical machine consists of the stationary part, called the stator, and cylindrical rotating part, referred as the rotor. It consists of two or more sources of magnetic excitation, which can be an electrical coils or permanent magnets, coupled magnetically by means of the magnetic circuit. The magnetic circuitry consists of the stator, air gap and rotor.

The modelling of a motor consisting of n stator and rotor windings is as follows:

$$\frac{d\boldsymbol{\lambda_s}}{dt} = \mathbf{u_s} - \mathbf{R_s i_s} \tag{3.61}$$

on stator

$$\frac{d\boldsymbol{\lambda_r}}{dt} = \mathbf{u_r} - \mathbf{R_r i_r} \tag{3.62}$$

on rotor $\boldsymbol{\lambda_s}^T = [\lambda_{s1}\, \lambda_{s2}\, \ldots \lambda_{sn}]$ and $\boldsymbol{\lambda_r}^T = [\lambda_{r1}\, \lambda_{r2}\, \ldots \lambda_{rn}]$. It can be expressed as $\boldsymbol{\lambda_s} = \mathbf{L_{ss}}\mathbf{i_s} + \mathbf{L_{sr}}\mathbf{i_r}$ and $\boldsymbol{\lambda_r} = \mathbf{L^T_{sr}}\mathbf{i_r} + \mathbf{L_{rr}}\mathbf{i_r}$

where $\mathbf{L_{ss}}$, $\mathbf{L_{rr}}$ are the self inductances matrices of the stator and rotor coils respectively and $\mathbf{L_{sr}}$ is the mutual inductance matrix between the stator and rotor coils.$\mathbf{i}_s^T = [i_{s1}\, i_{s2}\, \ldots i_{sn}]$ is stator current vector, $\mathbf{i}_r^T = [i_{r1}\, i_{r2}\, \ldots i_{rn}]$ is rotor current vector, $\mathbf{u}_s^T = [u_{s1}\, u_{s2}\, \ldots u_{sn}]$ is the stator input voltage vector, $\mathbf{u}_r^T = [u_{r1}\, u_{r2}\, \ldots u_{rn}]$ is the rotor input voltage vector, $\mathbf{R_s} = diag[R_s]_{n\times n}$ is diagonal stator resistance matrix, $\mathbf{R_r} = diag[R_r]_{n\times n}$ is diagonal stator resistance matrix.

In order to use this model, the flux linkage $\boldsymbol{\lambda}$ and the resistance matrix $\mathbf{R}$ of the stator and rotor must be calculated. The flux linkage is equivalent to the calculation of the total inductance of the stator and rotor coils. The total inductance is a sum of self and mutual inductances of the coils. Self inductance of a coil is the ratio of the flux linked by a coil to the current flowing in it, whereas mutual inductance is the ratio of the flux linked by one coil due to current flowing in a second coil with all other currents being zero including in the coil for which the flux linkages are being determined.

The self and mutual inductances affect the torque generated in an electrical machine. The study of the electromagnetic torque generation reveals that the torque generated in the electrical machines is the result of the change of the self-inductance and/or mutual inductances as a function of the angular position of the rotor. The configuration of the magnetic circuitry of electrical machines determines the dependence of the inductances of the coils, located at the stator and rotor structures, as function of the angular displacement of the rotor. In a machine having uniform air gap, self inductance of any coils situated on the stator or the rotor is independent of the rotor angular position. The mutual inductances between stator and rotor coils depend on the rotor angular position. The torque generated is given by

$$T_e = K_1(\boldsymbol{\lambda_r} \times \boldsymbol{\lambda_s}) = K_2(\boldsymbol{\lambda_r} \times \mathbf{i_s}) = K_3(\mathbf{i_r} \times \boldsymbol{\lambda_s}) \tag{3.63}$$

where K_1, K_2, K_3 are torque constants.

The mechanical motion equation is same as equation 3.60.

As the mutual inductances are dependent on the position of the rotor coils with

respect to the stator coils, it is time dependent. This leads to a complex set of equations which are difficult to analyze. A transformation of the variables can help simplify these equations and also removes the time varying inductances. This topic is discussed in the next section.

3.4 Reference frame transformations

Consider an electric machine having its input voltage vector $\mathbf{u}^T = [u_1\, u_2\, \ldots u_m]$ and input current vector, $\mathbf{i}^T = [i_1\, i_2\, \ldots i_m]$. Let $\mathbf{A}$ be the matrix which will cause the variable transformation, given by, $\mathbf{u} = \mathbf{A}\mathbf{u}'$, $\mathbf{i} = \mathbf{A}\mathbf{i}'$ where $\mathbf{u}'$ and $\mathbf{i}'$ represent the new variables.

Since both, the original and the transformed variables are describing the same set of equations, the power must be the same regardless of the variables used to describe it. So we can write:

$$P = \mathbf{i}^T\mathbf{u} = (\mathbf{A}\mathbf{i}')^T(\mathbf{A}\mathbf{u}') = (\mathbf{i}')^T\mathbf{A}^T\mathbf{A}\mathbf{u}' \tag{3.64}$$

$\mathbf{E} = \mathbf{A}^T\mathbf{A}$, $\mathbf{E}$ is unitary matrix then the selected transformation keeps the power invariant in the form.

Substituting this is the general equation, we get,

$$\frac{d\mathbf{L}\mathbf{A}\mathbf{i}'}{dt} + \mathbf{R}\mathbf{A}\mathbf{i}' = \mathbf{A}\mathbf{u}' \tag{3.65}$$

Taking derivatives and multiplying by $\mathbf{A}^{-1}$,we get

$$\mathbf{L}'\frac{d\mathbf{L}\mathbf{i}'}{dt} + [(\frac{\partial\mathbf{L}}{\partial\theta})'\frac{d\theta}{dt} + \mathbf{A}^{-1}\mathbf{L}\frac{d\mathbf{A}}{dt}]i' + \mathbf{R}'\mathbf{i}' = \mathbf{u}' \tag{3.66}$$

with $\mathbf{L}' = \mathbf{A}^{-1}\mathbf{L}\mathbf{A}$

$$\frac{\partial\mathbf{L}'}{\partial\theta} = \mathbf{A}^{-1}\frac{\partial\mathbf{L}}{\partial\theta}\mathbf{A} \tag{3.67}$$

The generated torque can be expressed as:

$$T_e = 0.5(\mathbf{i}')^T\mathbf{A}^{-1}\frac{\partial\mathbf{L}}{\partial\theta}\mathbf{A}\mathbf{i}' = 0.5(\mathbf{i}')^T\frac{\partial\mathbf{L}}{\partial\theta}\mathbf{i}' \tag{3.68}$$

As it can be seen, the torque generated is unaffected by the transformation.

In the mathematical models of the machines presented, the stator variable were presented in the (a,b,c) co-ordinate frame, stationary with respect to the stator coils and

the rotor variables were presented in the (a,b,c) co-ordinate frame, stationary with respect to the rotor coils. The two co-ordinate frames are shifted by the rotor angular position θ.

It would be convenient if all the equations are described in the same co-ordinate system. To achieve this, the stator or rotor or both set of variables need to be transformed. We can obtain three types co-ordinate frames using tranformations, i.e. co-ordinate frame stationary with respect to the stator, co-ordinate frame stationary with respect to the rotor, co-ordinate frame non-stationary with respect to the stator or rotor. The co-ordinate frame that is stationary with respect to the rotor frame will be analysed in this study. This transformation is known as Clark-Park transformation and the new transformed frame is called the direct-quadrature co-ordinate frame or simply (d,q) co-ordinate frame. Clark-Park transformation is a two step process involving a Clark and a Park transform. It is discussed in detail in section 3.6.

In this previous section we derived the force generated and a general dynamical model of an n input electrical machine. We also discussed reference frame transformations. In the following sections, the theory and models of permanent magnet DC motor, Permanent Magnet Synchronous Motor(PMSM) and Induction Motor(IM) will be studied.

3.5 DC motor

A brushed DC motor is the simplest of all the motors and has many large and small scale applications in the industry. These are easy to control and can be used for a large speed range with high efficiency. Major elements of a DC machine are stator that carries either permanent magnet or field winding and the rotor with a commutator which passes the current into the rotor windings are shown in Figure 3.9

The force on the conductor is given by Lorentz force, f

$$f = I(\mathbf{l} \times \mathbf{B}) = IlBsin(\theta) \tag{3.69}$$

Where $\mathbf{B}$ is the intensity of the magnetic field, $\mathbf{l}$ is the length of the conductor, I is the value of the current flowing in the conductor and θ is the angle between the conductor and the magnetic field.

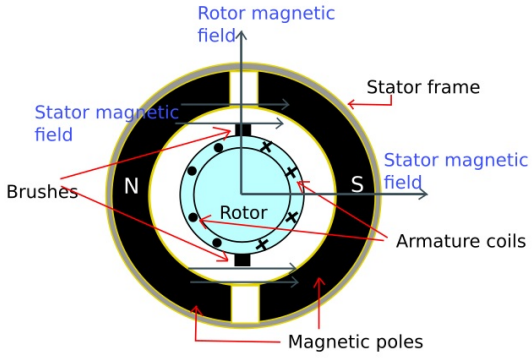

(a) DC motor stator and rotor

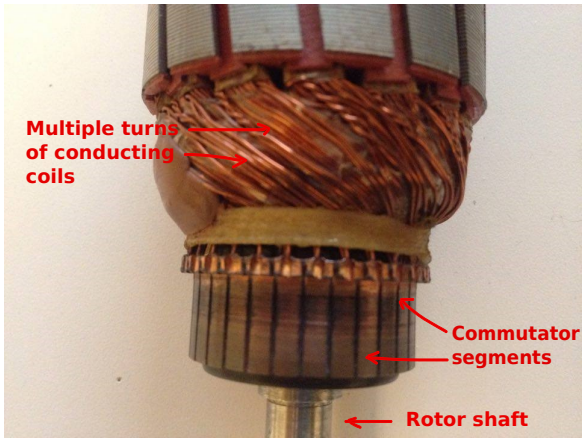

(b) DC motor rotor

Figure 3.9: Close up view of DC motor stator and rotor

Commonly there are multiple copper segments with multiple turns of coils between each of them. When the coils are rotating in the magnetic field, the flux associated with each coil is also changing. This changing flux causes a voltage to be induced in the rotor coil. According to Lenz's law this voltage is in opposition to the voltage that causes the current flow through the coils and is called back-emf.

The DC motor can be modelled using the following equations

$$\frac{d\lambda_r}{dt} = u_r - K_e w - R_r i_r \tag{3.70}$$

$$\lambda_r = L_r i_r \tag{3.71}$$

where λ_r is the rotor flux, L_r is the rotor coil inductance, i_r is the current in the rotor coils, K_e is the back emf constant, w is the speed of the rotor, R_r is the rotor coil resistance, and u_r is the input voltage at the brushes.

The torque expression for a permanent magnet DC motor can be derived from the general torque equation 3.57. The stator magnets are responsible for the generation of the stator flux whereas the current flowing through the rotor coils generates the rotor flux. The stator and rotor fluxes are always orthogonal to each other due to the construction of the DC motor. This fact can also be seen in Figure 3.9. The torque is given by

$$T_e = K_T \lambda_s i_r \tag{3.72}$$

The torque experienced by a coil is proportional to the current flowing through it, hence the presence of multiple turns of coils results in a higher current in a particular slot of the rotor leading to a higher torque.
The mechanical motion equation is same as that of equation 3.60.

3.6 Permanent Magnet Synchronous Motor

Synchronous motors differ from the DC motors in the construction and input power supply. Synchronous motors like DC motors consist of stator, rotor with the difference that the rotor has permanent magnets instead of the stator. Moreover it uses AC power as opposed to DC for the DC motors.

Synchronous machines are the source of almost all of the electric power generated in the world so far. They can be operated either as a generator or a motor. It operates as a motor when a 3-phase supply is given to the stator. The Permanent Magnet Synchronous Motor (PMSM) has a permanent magnet mounted on the rotor and can be classified as surface PMSM and interior PMSM based on the way the magnets are placed on the rotor. This thesis considers Surface mounted PMSM. The rotor of the PMSM rotates with the same speed as the magnetic field of the stator, hence the name synchronous motor. The speed of a synchronous motor is dependent on the frequency of the supply and does not change with changes in the load. Hence it can be used where constant speed output is required.
Here we will be concentrated on the 3 phase permanent magnet synchronous machine as sketched in Figure 3.10.

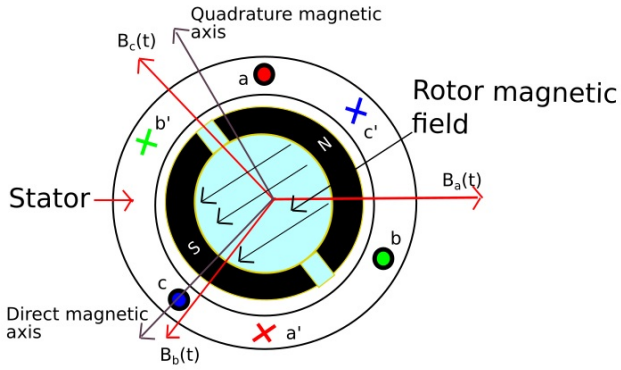

(a) PMSM stator and rotor assembly

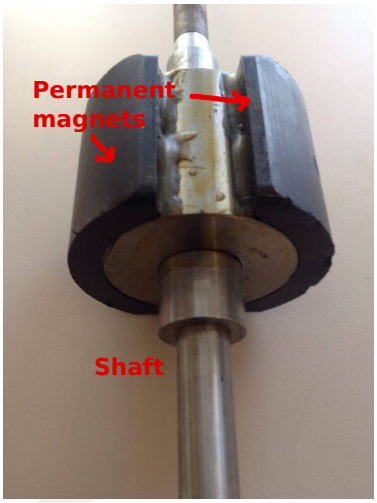

(b) Two pole Rotor

Figure 3.10: PMSM stator and rotor

The three phase stator coils can be connected in a Y or Delta format and are spaced 120 degrees in the stator. When a sinusoidal current flows through the coil a sinusoidal magnetomotive force (mmf) is generated in the coil whose amplitude and direction is dependent on the instantaneous value of the current flowing through the coil. Each of the three phase coils will generate similar mmf's but will be shifted by 120 degrees with respect to each other. The resultant of these mmf's is vector with constant amplitude that is rotating at a constant angular velocity. The magnetic flux corresponding to this mmf will interact with the rotor flux to produce torque. The rotor flux tries to align itself with the stator flux. Whenever the rotor flux rotates in synchronism with the stator flux, constant torque is produced. The torque is given by

$$T_e = K_1(\boldsymbol{\lambda_r} \times \boldsymbol{\lambda_s}) = K_2(\boldsymbol{\lambda_r} \times \mathbf{i_s}) \tag{3.73}$$

where where $\boldsymbol{\lambda_r}$ is the rotor flux vector due to the permanent magnet, $\boldsymbol{\lambda_s}$ is the stator flux vector due to the stator currents, $\mathbf{i_s}$ and K_1, K_2 are torque constants.

The velocity with which the rotor rotates is dependent on the number of poles of the stator and is given by,

$$\mathbf{w_m} = \frac{2}{P}\mathbf{w_e} \tag{3.74}$$

Where P is the number of poles of the stator.

Similarly the mechanical angle and the electrical angle are also related as follows:

$$\boldsymbol{\theta_m} = \frac{2}{P}\boldsymbol{\theta_e} \tag{3.75}$$

The PMSM can be modelled using the following equations

$$\frac{di_a}{dt} = -i_a\frac{R}{L} - e_a\frac{1}{L} + u_a\frac{1}{L} \tag{3.76}$$

$$\frac{di_b}{dt} = -i_b\frac{R}{L} - e_b\frac{1}{L} + u_b\frac{1}{L} \tag{3.77}$$

$$\frac{di_c}{dt} = -i_c\frac{R}{L} - e_c\frac{1}{L} + u_c\frac{1}{L} \tag{3.78}$$

where R and L are the coil resistances and inductances of each of the three coils respectively, i_a, i_b, i_c and u_a, u_b, u_c are the phase currents and voltages respectively. e_a, e_b, e_c are the induced emf components given by

$$e_a = \frac{d\lambda_{ma}}{dt} \tag{3.79}$$

$$e_b = \frac{d\lambda_{mb}}{dt} \tag{3.80}$$

$$e_c = \frac{d\lambda_{mc}}{dt} \tag{3.81}$$

where λ_{ma}, λ_{mb}, λ_{mc} are the flux components generated by the permanent magnet, λ_m, along the three stator coils. They are given $\lambda_{ma} = \lambda_m cos(\theta_e)$, $\lambda_{mb} = \lambda_m cos(\theta_e - \frac{2\pi}{3})$, $\lambda_{mc} = \lambda_m cos(\theta_e + \frac{2\pi}{3})$. Now, we can write e_a, e_b, e_c as follows

$$e_a = -\lambda_m w_e sin(\theta_e) \tag{3.82}$$

$$e_b = -\lambda_m w_e sin(\theta_e - \frac{2\pi}{3}) \tag{3.83}$$

$$e_c = -\lambda_m w_e sin(\theta_e + \frac{2\pi}{3}) \tag{3.84}$$

From equations 3.79-3.81, it can be seen that the induced emf in the coils is dependent on the rotor speed. This implies that the voltage equations 3.76-3.78 are time dependent and complex to analyze. Hence, to reduce the complexity, the co-ordinate frame is transformed from a 3-phase (a,b,c) co-ordinate system to a (d,q) co-ordinate frame which appears stationary with respect to the rotor. This transformation, also called

as the Clark – Park transformation is a two step process involving a Clark and a Park transform.

A Clark transform is used to transform a 3-phase stationary frame of reference i.e. (a,b,c) co-ordinate frame to a 2-phase stationary frame of reference (α, β) co-ordinate frame as shown in Figure 3.11. This frame of reference is then transformed to a 2-phase rotating frame i.e. (d,q) co-ordinate frame using Park transform. These transformations require the position of rotor flux to do the transformation accurately.

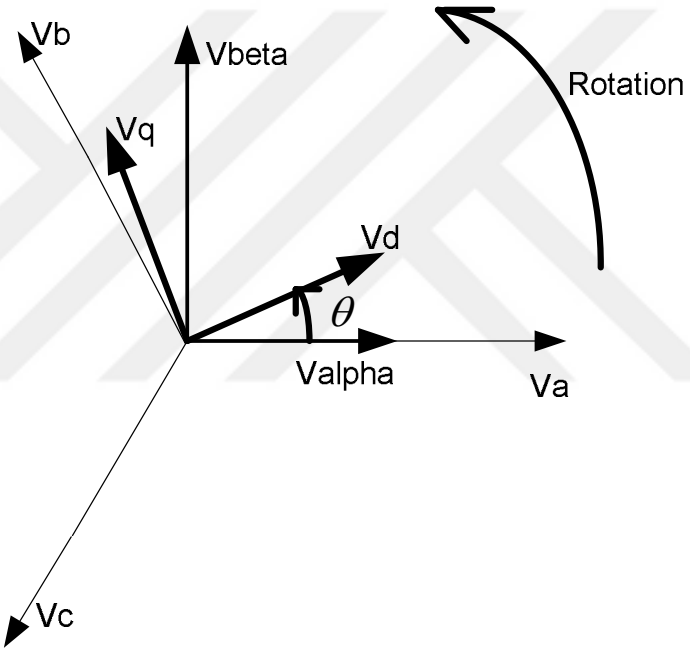

Figure 3.11: (d,q) co-ordinate frame with respect to (a,b,c) and (α, β) co-ordinate frame

Clarke Transform:

$$\mathbf{T}_{\alpha,\beta}^{a,b,c} = \begin{bmatrix} u_\alpha \\ u_\beta \end{bmatrix} = \frac{2}{3} \begin{bmatrix} 1 & -\frac{1}{2} & -\frac{1}{2} \\ 0 & \frac{\sqrt{3}}{2} & -\frac{\sqrt{3}}{2} \end{bmatrix} \begin{bmatrix} u_1 \\ u_2 \\ u_3 \end{bmatrix}$$

where $\mathbf{T}_{\alpha,\beta}^{\mathbf{a,b,c}}$ is the Clark transformation matrix.

Park transform: The axis stationary co-ordinate system is then transformed to a rotating co-ordinate system using the Park transform

$$\mathbf{T}_{d,q}^{\alpha,\beta} = \begin{bmatrix} u_d \\ u_q \end{bmatrix} = \begin{bmatrix} cos(\theta) & sin(\theta) \\ -sin(\theta) & cos(\theta) \end{bmatrix} \begin{bmatrix} u_\alpha \\ u_\beta \end{bmatrix}$$

Where θ is the position of rotor flux and $\mathbf{T}_{d,q}^{\alpha,\beta}$ is the Park transformation matrix.

After applying these transformations the time varying inductances become time independent i.e. constant. Moreover, it is also helpful in speed control of AC machines. Its application in speed control of AC machines is discussed after the derivation of the model in the (d,q) co-ordinate frame as well as in Chapter 5.

Applying Clark transform to the voltage equations of 3.76-3.78 we get

$$\frac{di_\alpha}{dt} = -i_\alpha \frac{R}{L} - e_\alpha \frac{1}{L} + u_\alpha \frac{1}{L} \tag{3.85}$$

$$\frac{di_\beta}{dt} = -i_\beta \frac{R}{L} - e_\beta \frac{1}{L} + u_\beta \frac{1}{L} \tag{3.86}$$

where $e_\alpha = -\lambda_m w_e sin(\theta_e)$ and $e_\beta = \lambda_m w_e cos(\theta_e)$.

e_α, e_β are the induced emf, i_α, i_β are the stator currents and u_α, u_β are the stator voltages in the (α, β) co-ordinate frame. Now applying the Park transform to equations 3.85,3.86, we get the motor model in the (d,q) co-ordinate frame.

$$\frac{di_d}{dt} = -i_d \frac{R}{L} - w_e i_q + u_d \frac{1}{L} \tag{3.87}$$

$$\frac{di_q}{dt} = -i_q \frac{R}{L} - w_e i_d - \lambda_m w_e \frac{1}{L} + u_d \frac{1}{L} \tag{3.88}$$

where i_d, i_q are the stator currents, u_d, u_q are the stator voltages in the (d,q) co-ordinate systems. The term $\lambda_m w_e = e_q$ is the q component of the induced emf due to the permanent magnet and d component $e_d = 0$.

An important point to be noted from equations 3.87,3.88 is that if we make $i_d = 0$, the equations are the same as that of the permanent magnet DC motor. This feature of the transformation is used in the speed control applications of AC motors.
The torque equation in the (d,q) co-ordinate frame is given by

$$T_e = K_t i_q \tag{3.89}$$

where $K_t = 1.5P\lambda_m$, P being the number of poles of the stator. The mechanical motion equation is the same as equation 3.60.

3.7 Induction Motor

The induction motors are considered the work horses of the motion industry as they are used in numerous applications. The induction motor can be classified into two types depending upon the rotor construction as: squirrel cage or wound rotor. The squirrel cage type is particularly most widely used motor for industrial applications. In this thesis, experiments are done over the squirrel cage type induction motor. The

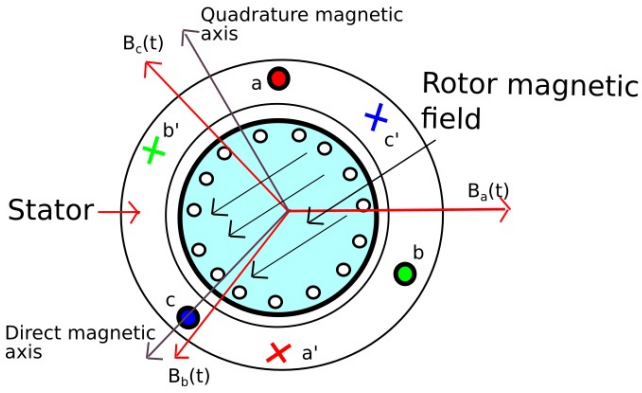

(a) Induction motor stator and rotor

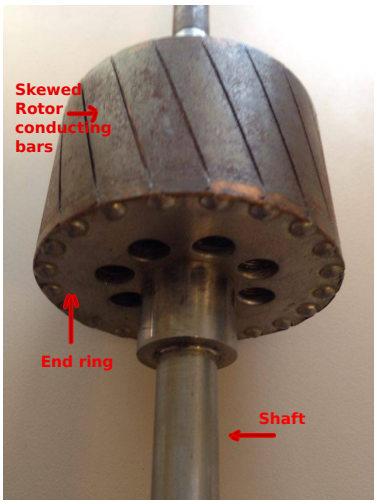

(b) Squirrel cage rotor

Figure 3.12: Induction motor

stator of an induction motor has the same construction as that of a permanent magnet synchronous motor. The difference between the two is the rotor construction. The

PMSM rotor has magnets attached to its shaft whereas the squirrel cage rotor is made up of aluminum or copper bars. These bars are short circuited at the two ends by aluminum or copper end rings. The torque can be given by

$$T_e = K_1(\boldsymbol{\lambda_r} \times \boldsymbol{\lambda_s}) = K_2(\boldsymbol{\lambda_r} \times \mathbf{i_s}) \tag{3.90}$$

where $\boldsymbol{\lambda_s}$ is the stator flux vector, $\boldsymbol{\lambda_r}$ is the rotor flux vector and $\mathbf{i_s}$ is the stator current vector and K_1, K_2 are torque constants.

The model of the induction motor in the (d,q) co-ordinate system is represented as follows:

$$\frac{di_d}{dt} = -\gamma i_d + \eta\beta\lambda_d + w_s i_q + \frac{u_d}{\sigma L_s} \tag{3.91}$$

$$\frac{di_q}{dt} = -\gamma i_q - w_s\beta\lambda_d - w_s i_d + \frac{u_q}{\sigma L_s} \tag{3.92}$$

$$\frac{d\lambda_d}{dt} = -\eta\lambda_d + \eta L_h i_d \tag{3.93}$$

$$\frac{d\rho}{dt} = w_s + \eta L_h \frac{i_q}{\lambda_d} \tag{3.94}$$

$\eta = \frac{R_r}{R_s}$, $\sigma = 1 - \frac{{L_h}^2}{L_s L_r}$, $\beta = \frac{L_h}{\sigma L_s L_r}$, $\gamma = \frac{1}{\sigma L_s}(R_s + \frac{{L_h}^2}{{L_r}^2} R_r)$

where R_s,R_r are the stator and rotor resistances, L_s, L_r,L_h is the stator, rotor and manual inductance, i_d,i_q are the (d,q) axis stator currents, λ_d is the d component of the rotor flux and u_d, u_q are the (d,q) axis voltages.

The torque is given by:

$$T_e = 1.5P\frac{L_h}{L_r}\lambda_d i_q \tag{3.95}$$

The mechanical motion equation is the same as equation 3.60. The simulation models of these motors can be found in Appendix - B

Chapter 4

Mechatro Lab New components

The achievement of the objective set in Chapter 2 requires development of the additional hardware and software components. In this chapter we will give short description of these components and their usage in overall system.

1. Measurement Unit: The current and mechanical co-ordinate measurement (position and velocity) are added to the setup.

   (a) Current measurement: The current measurements are done using LTS 6 NP. It can measure DC, AC, pulsed currents with isolation between the high power and electronic circuitry. The range of operation can also be changed to 2A or 3A by changing the way in which its pins are connected. The current sensor gives an analog output between 0-5V depending on the current flowing through it. The analog output is given to the Analog to digital converter of the micro-controller. The current sensors are integrated inside the power converter board.

Characteristics	Value
Primary current (rms)	6A
Load resistance	$> 2k\Omega$
Accuracy	$\pm 0.2\%$
Supply voltage	5V

Table 4.1: Characteristics of LTS6-NP current sensor

(b) Rotary Encoder: WDG 50B encoder is used for position and speed measurements. It is an optical rotary incremental encoder with a resolution of 1024 pulses per revolution. It's output is given to the Quadrature Encoder unit of the microcontroller.

Characteristics	Value
Max. pulses per revolution(PPR)	2500
Max. operating speed	12000rpm
Channels	AB, ABN, inverted AB

Table 4.2: Characteristics of rotary encoder

4.1 TMS320F28335 controller

The TMS320F28335 is selected as the core device enabling control and data processing in the Mechatro Lab. The microcontroller, TMS320F28335 is part of the C2000 Delfino 32-bit microcontroller series. This series of microcontrollers are designed for advanced closed loop control applications.

TMS320F28335 is a 32-bit Digital Signal Controller with processor speeds up to 150MHz. It is based on 32-bit fixed point architecture but also includes a single precision floating point unit. It has 256Kw of on-chip flash memory and a code security module to prevent reverse engineering of the control system. The following features of the controller

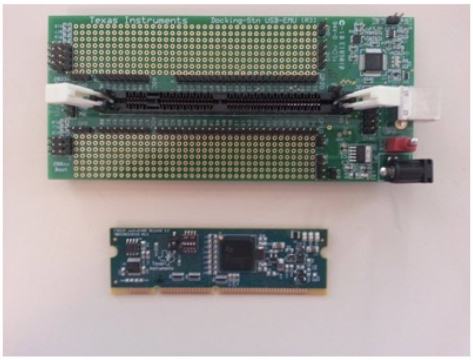

Figure 4.1: TMS320F28335 micro controller

will be utilized in this study.

ePWM: The Enhanced Pulse Width Modulation module can be used to generate independent as well as complementary PWM signals. This module can be operated in two modes 1) Standard 16 bit mode and 2) 24-bit high resolution mode. The ePWM registers are supported by DMA to reduce the overhead for servicing this peripheral.

32-bit CPU timers: The controller consists of three 32-bit timers. Timer 0 and 1 are for general purpose use whereas timer 2 is reserved for Real Time OS applications. The timers consist of 32 bit registers which count down from a set value and generate an interrupt when the count value reaches zero. The timer register are reloaded with the count value automatically on reaching zero.

ADC: The controller also consists of a 12-bit ADC with conversion time of 80ns. There are 16 channels which can be converted using two sample and hold circuits in simultaneous or cascaded modes. The ADC registers are also supported by the DMA to reduce the overhead for servicing this peripheral.

eQEP: The Enhanced Quadrature Encoder Module is used to measure the position, direction and speed of a rotating machine. It supports both high and low speed measurements using a 32-bit timer. For low speed measurement the intervals between two consecutive encoder pulses is measured by counting the number of clock pulses, hence providing accurate low speed measurements.

4.1.1 Programming environment

The implementation of the control algorithms is done using Texas Instruments(TI) software. The software is called Code Composer Studio, CCStudio or CCS. Code Composer Studio is an integrated development environment (IDE) and is used to develop and debug applications for the TI's embedded processors. The coding can be done in C/C++ and Assembly language. It can be used for all families and variations of the TI's digital signal processors. The software is used in the initial phase in which there are frequent changes to the software. Once the testing was complete the code was stored in flash memory so that it operates directly on power on.

4.2 Power converter board

The three phase DC to AC converter is a core power conversion unit of the Mechatro Lab. It design enables the usage as

1. Power electronic device with LC filter
   (a) DC-DC converter
   (b) Single phase DC to AC converter
   (c) Three phase DC to AC converter
2. Converter to supply DC or AC (single or three phase)machine

The structure of the converter is shown in Figure 4.2.

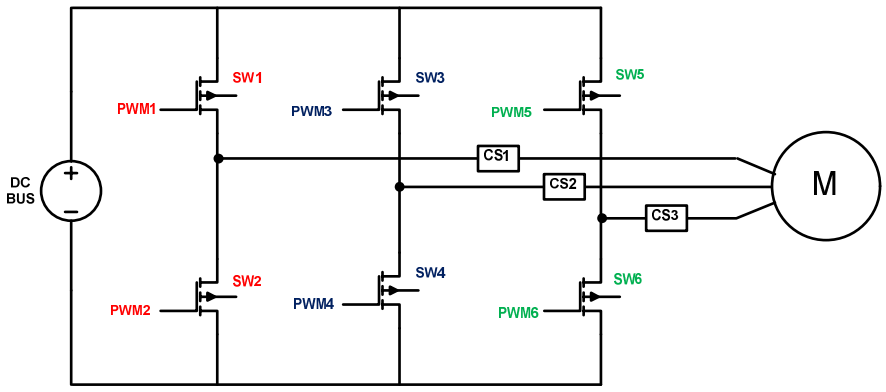

Figure 4.2: Structure of the converter

The three branches are the same and are designed using the following components:

1. MOSFET: IRF630 is used as the switches. Its characteristics are as shown below:

Characteristics	Value
Drain-Source voltage	200V
Gate-Source voltage	$\pm 20V$
Continuous drain current	9A
Max Power dissipation	74W

Table 4.3: Characteristics of IRF630 MOSFET

2. Diode: SR5100 is used as the flyback diode. Its characteristics are as shown below:

Characteristics	Value
Max recurrent peak reverse voltage	100V
Max DC blocking voltage	100V
Max average forward rectified current	5A

Table 4.4: Characteristics of SR5100 Diode

3. Motor driver IC: It provides driving signals for each branch

Characteristics	Value
High side floating supply offset voltage	600V
Turn-on propagation delay	680ns
Turn-off propagation delay	150ns
Gate drive supply range	10-20V
Deadtime	520ns

Table 4.5: Characteristics of IR2104 half bridge driver

4. Optocoupler: It is used for isolating the controller board from the converter board.

Characteristics	Value
Max Input power dissipation	45mW
Average input current	25mA
Input forward voltage	1.5V

Table 4.6: Characteristics of opto-coupler

The prototype converter is shown in Figure 4.3.

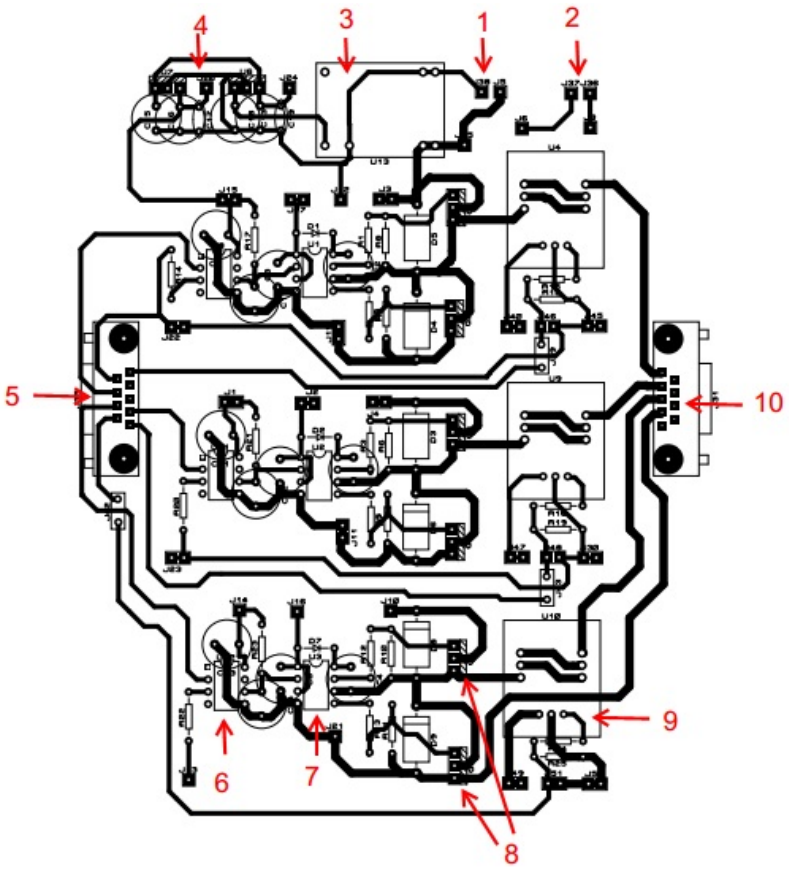

Figure 4.3: Power converter board layout

1 - DC Bus voltage (0-60V), 2 - Current sensor supply voltage - 5V, 3 - 60V to 15V DC-DC converter, 4 - Power supply for the optocoupler and the half bridge driver IC (5V and 15V respectively), 5 - Connections between the micro-controller and the board through a DB9 cable, 6 - Optocoupler IC, 7 - Half bridge driver IC, 8 - MOSFET switch, 9 - Current Sensor, 10 - DB9 connector having the 3 phase lines and a board ground line.

The basic technical characteristic of the converter are:

1. Supply voltage 200V DC
2. Per phase Current capacity of 9A.
3. Galvanic isolation.

4.3 Graphical user interface

Any user PC with MATLAB installed on it can be used for overall control of the Mechatro Lab and establish a GUI that allows:

1. Running simulation with own or prepared models
2. Access to DSP microcontroller and execution of its own or predefined algorithms
3. Change parameters and collect measurement data

The users can interact with the micro-controller using the user interface developed in MATLAB. The GUI is developed using the GUIDE(Graphical user interface development environment) feature of MATLAB. The GUI interacts with the micro-controller using serial communication.
The motor selection is performed in the main GUI window. The motor specific interface can be opened by clicking on the push buttons having the motor name.

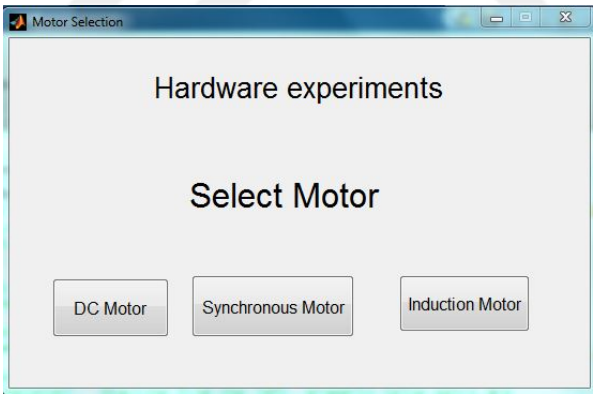

Figure 4.4: Main GUI window

In these interfaces, the users can enter different reference speed inputs and observe the speed and current response. The users can also enter the PID gain parameters in the boxes and observer the its effect on the speed and current response.

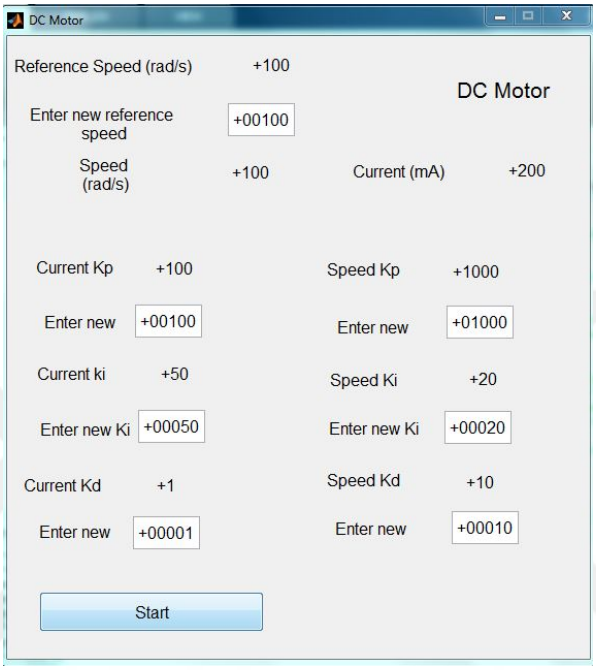

Figure 4.5: DC Motor GUI

Chapter 5

Electric Machine Control Design and Simulation

In this chapter we will be showing the basic algorithms developed for control of DC and AC machines as examples on how basic operation of Mechatro lab with new DSP controller can be used. The work shown in this chapter is a background for the development of the DSP code and experimentation on velocity control of different electrical machines.

The Speed control techniques of DC and AC motors are discussed in the following sections. There are various techniques which are applied to the DC and AC motors. The most simple control technique which can be applied to a DC motor is the PID controller [38]. The PID controllers are used extensively in industries for speed control of DC motor [39][40]. PID controllers are popular mainly due to its simplicity. It requires the knowledge of the parameters of the system to calculate the proportional-integral-derivative gains. However, it is not suitable if the system is non-linear[41][42].

5.1 Speed control of DC motor

In a permanent magnet DC motor the stator and rotor fluxes are orthogonal by machine construction thus for permanent magnet machine with constant stator field the torque can be controlled by changing the rotor current.

A block diagram used in speed control of DC motor is shown in Figure 5.1

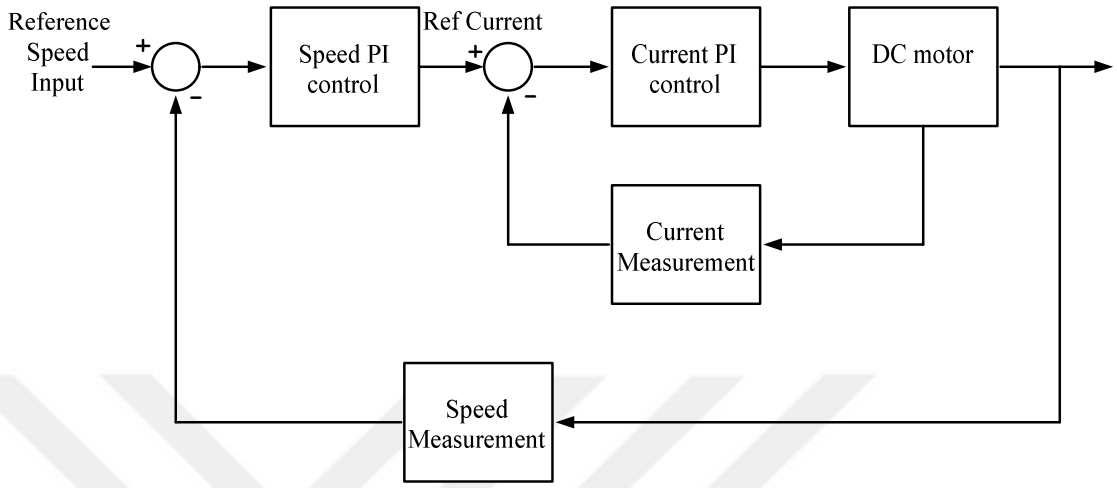

Figure 5.1: Speed Control block diagram of a DC motor

The outer speed PI controller generates a reference current depending upon the difference in the actual and reference speed. This reference current is responsible to generate the necessary torque to achieve the desired speed. The reference current is then compared with the motor current and a controller is applied to the error between them. The output of this PI controller is the voltage applied to the terminals of the DC motor. This control technique is called cascaded control technique

An important feature of the current control loop is that we can put a saturation limit to the reference current, which is the maximum rated current of the motor. If the reference speed is changed in such a way that the reference current goes beyond the rated current, the saturation condition will maintain the reference current within the maximum current rating of the motor.

In the following section, the PI controller is designed and the gains obtained are used in the Simulink simulation. The control system is designed on the model of equations 3.60, 3.70-3.72 developed in Chapter 3.

The Laplace transform taking u as a control input and $K_e w$ as disturbance leads to an open loop transfer function as

$$\frac{i(s)}{u(s)} = \frac{1}{(Ls + R)} \tag{5.1}$$

Selecting PI controller as

$$C_1 = K_p + \frac{K_i}{s} \tag{5.2}$$

leads to closed loop transfer function as

$$T_{ci} = \frac{C_1 T_{oi}}{(1 + C_1 T_{oi})} \tag{5.3}$$

Let $a(s)$ represent the characteristic polynomial of the above transfer function. It is given by

$$a(s) = 1 + C_1 T_{oi} \tag{5.4}$$

Simplifying Equation 5.4, we get

$$a(s) = s^2 + \frac{(R + K_p)}{L} s + K_i \tag{5.5}$$

Substituting the parameters of the motor, the characteristic equation can be written as

$$a(s) = s^2 + \frac{(11.2 + K_p)}{0.028} s + K_i \tag{5.6}$$

Applying the Routh's Stability criterion We get $K_i > 0$ and $K_p > -11.2$.
Using these equations the values of $K_p = 100$ and $K_i = 10$ were used in the simulation. The outer control loop implemented as below

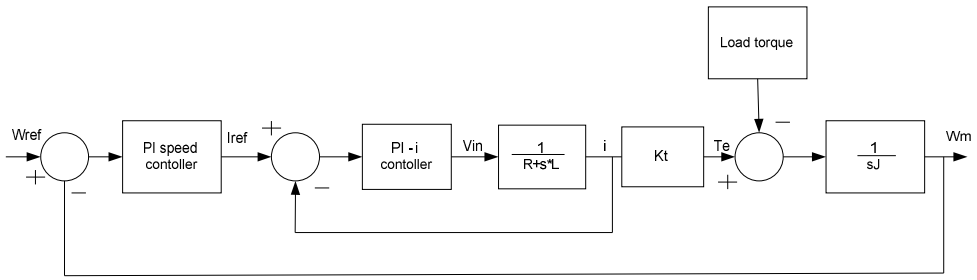

Figure 5.2: Outer control loop: DC motor Speed Control

The PI controller for the outer loop can be written as

$$C_2 = K_p + \frac{K_i}{s} \tag{5.7}$$

$$T_{ow} = \frac{C_2 T_{ci} K_t}{sJ} \tag{5.8}$$

$$T_{cw} = \frac{T_{ow}}{(1 + T_{ow})} \tag{5.9}$$

The characteristic equation is given as below

$$a(s) = s^3(100LK_pK_t)+s^2(100RK_pK_t+100LK_iK_t+10LK_pK_t)+s(10RK_pK_t+10LK_iK_t)+10RK_iK_t \tag{5.10}$$

Substituting the motor parameters, the equation can be simplified as below

$$a(s) = s^3(9K_p) + s^2(356K_p + 9K_i + 3LK_p) + s(3K_p + 0028K_i) + 35K_i \tag{5.11}$$

Applying the Routh's Stability criterion

We get the conditions as $K_i > 0.028K_p$ and $12250K_p^2 + 31.5K_pK_i - 31K_i < 0$.

Using these equations, the values of $K_p = 0.1$ and $K_i = 0.5$ gave good results in the simulation.

The results of using these gains are shown in the speed and current response in Figure 5.3. It can be seen that the speed and current follow their references within 50ms.

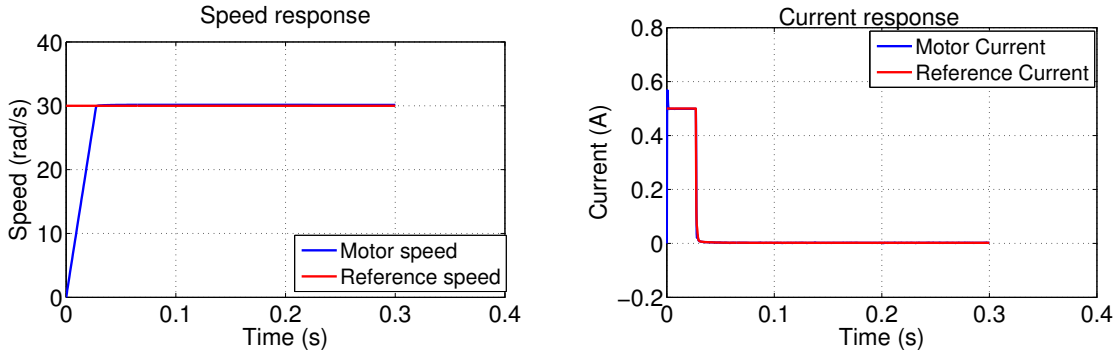

(a) Speed Response

(b) Current Response

Figure 5.3: DC Motor Simulation Speed reference : 0 to 30 rad/s

5.2 Speed Control of AC motors

The control algorithms of the AC motors are much more complicated than that of DC motors. The most popular and widely used speed control technique for AC motors

is Vector control or Field oriented control. It was introduced by Blaschke.F in early 1970's[43]. Inorder to implement this technique, rotor flux estimates are required. The rotor flux can be measured directly using a flux meter or can be estimated from the stator currents. These two separate methods lead to the classification as direct and indirect field oriented control respectively.

Scalar control or Volts per Hertz control is another control technique which can be applied to AC machines. In this technique the magnitude of the 3 phase voltage given to the motor is varied in proportion to the output speed required. It is a much simpler control technique than vector control. A comparative study of the scalar and vector control was done by Jisha et al[44]. They concluded that the transient behavior in vector control is better than that in scalar control. Although Vector control is more complex, its performance is much better than scalar control. Texas Instruments published documents on FOC of PMSM and IM, explaining the theory and a step by step implementation of the control technique[45][46].

The block diagram of field oriented control is shown in Figure 5.4. Projecting the dynamics of AC machines (Synchronous and IM) into the frame of reference with d-axis oriented along the rotor flux vector leads to dynamic decoupling of the machine dynamics similar as in DC machines. Then d-axis current controls the rotor magnetizing flux whereas the q-axis current controls the torque. They are then controlled separately as shown in Figure 5.4.

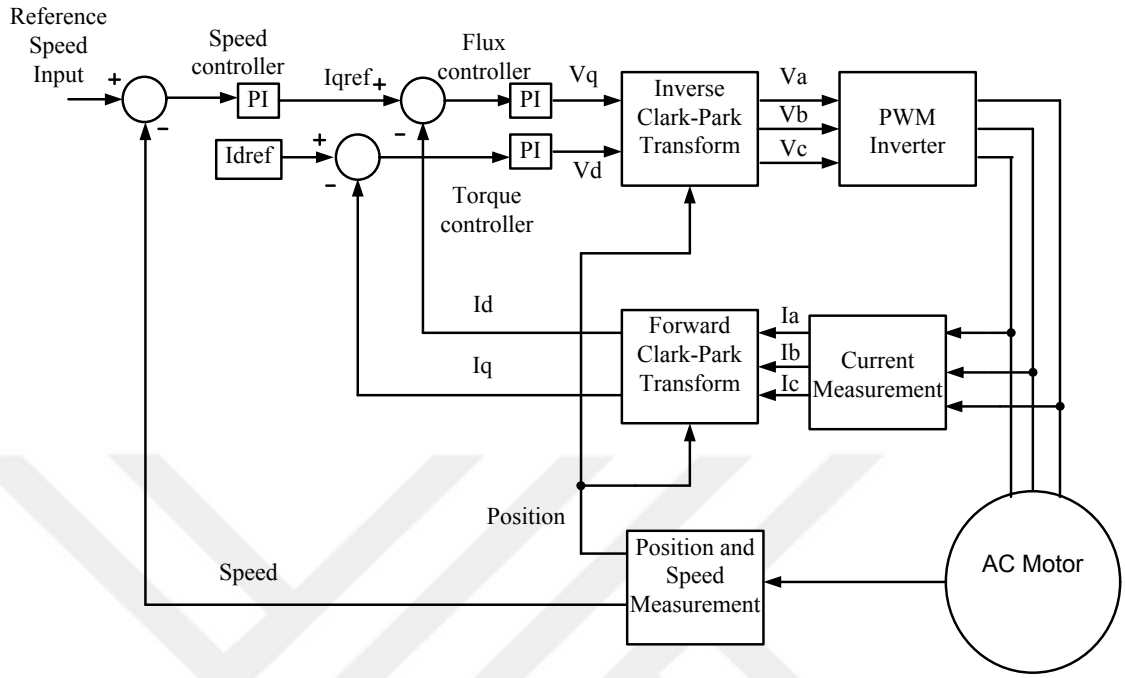

Figure 5.4: Field Oriented Control - Block Diagram

The outer PI loop generates i_{qref} depending upon the difference in the reference and actual speed. The i_d and i_q values are then compared with i_{dref} and i_{qref} values. In the PMSM, $i_{dref} = 0$, as the rotor magnets generate the magnetizing flux, hence there is no need to create a magnetizing flux from the stator flux. The torque depends only upon the q-axis current. Whereas in the case of induction machine, i_{dref} is decided based on the speed. Its torque is dependent upon the rotor flux as well as the q-axis current. A linear relation between the torque and the q-axis current can be established by maintaining a constant value of rotor flux. In this way, the torque can be controlled by controlling the q-axis current.

5.2.1 PMSM Control system design

The control system for PMSM is designed using equations 3.87-3.89 and 3.60. The inner control loop for the d and q axis currents is designed as follows

$$\frac{di_d}{dt} = \frac{u_d}{L} - \frac{Ri_d}{L} - w_e i_q \tag{5.12}$$

$$\frac{di_q}{dt} = \frac{u_q}{L} - \frac{Ri_q}{L} - w_e i_d - \frac{w_e \lambda_m}{L} \tag{5.13}$$

The non-linear terms in both the equations, namely $w_e i_q$ and $w_e i_d$ can be considered as disturbance, to be compensated by the controller.

Let $u_{dd} = u_d - w_e i_q$ and $u_{qq} = u_q - w_e i_d + \frac{w_e \lambda_m}{L}$.

Therefore

$$\frac{di_d}{dt} = \frac{u_{dd}}{L} - \frac{Ri_d}{L} \tag{5.14}$$

$$\frac{di_q}{dt} = \frac{u_{qq}}{L} - \frac{Ri_q}{L} \tag{5.15}$$

Taking Laplace transform

$$si_d(s) = \frac{u_{dd}(s)}{L} - \frac{R}{L} i_d \tag{5.16}$$

$$(sL + R) i_d(s) = u_{dd}(s) \tag{5.17}$$

$$T_{od} = \frac{1}{sL + R} \tag{5.18}$$

Similarly we can write

$$(sL + R) i_q(s) = u_{qq}(s) \tag{5.19}$$

$$\frac{i_q(s)}{u_{qq}(s)} = \frac{1}{sL + R} \tag{5.20}$$

$$T_{oq} = \frac{1}{sL + R} \tag{5.21}$$

Substituting the motor parameters, we get,

$$T_{od} = \frac{1}{0.4s + 16} = T_{oq} \tag{5.22}$$

Applying PI controller to the T_{od} and T_{oq}, we get,

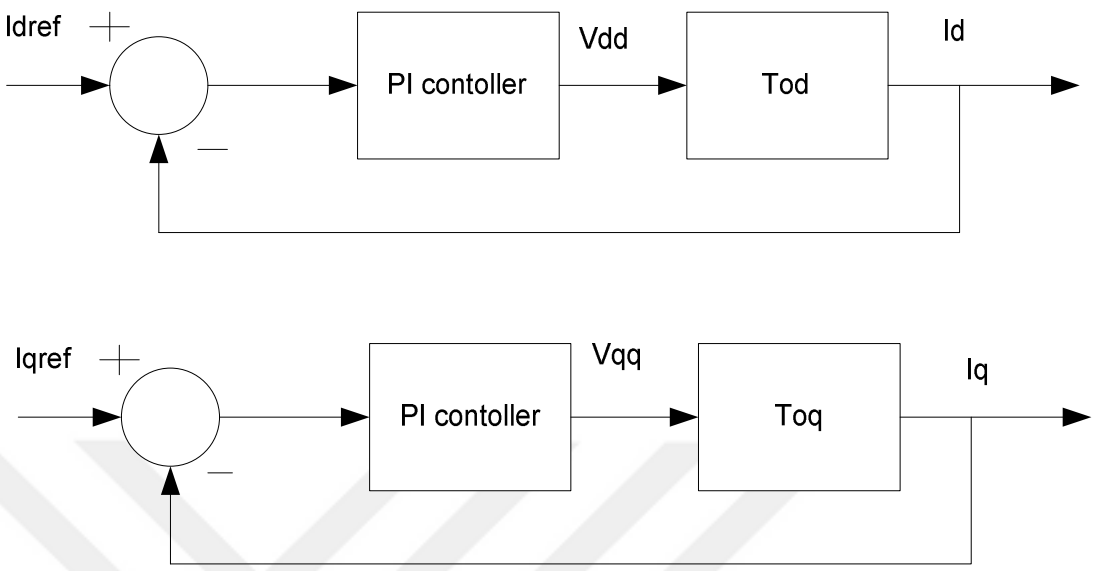

Figure 5.5: d and q axis current control loop: PMSM Speed Control

The closed loop transfer function is given by

$$T_{cd} = \frac{C_1 T_{od}}{1 + C_1 T_{od}} \tag{5.23}$$

Where, $C_1 = K_p + \frac{K_i}{s}$

The characteristic polynomial of the above transfer function is given by

$$a(s) = 1 + C_1 T_{od} \tag{5.24}$$

Substituting the values of C_1 and T_{od}, we get,

$$a(s) = s^2 + \frac{16 + K_p}{0.4} s + \frac{K_i}{0.4} \tag{5.25}$$

Applying the Routh's Stability criterion, we get $K_i > 0$ and $K_p > -16$.

The inner loop works satisfactorily for $K_p = 100$ and $K_i = 100$.

The same gains can be applied to T_{oq} .

The controller design for the outer speed loop is done as below

$$T_{ow} = \frac{C_2 T_{oq} 1.5 P \lambda_m}{sJ} \tag{5.26}$$

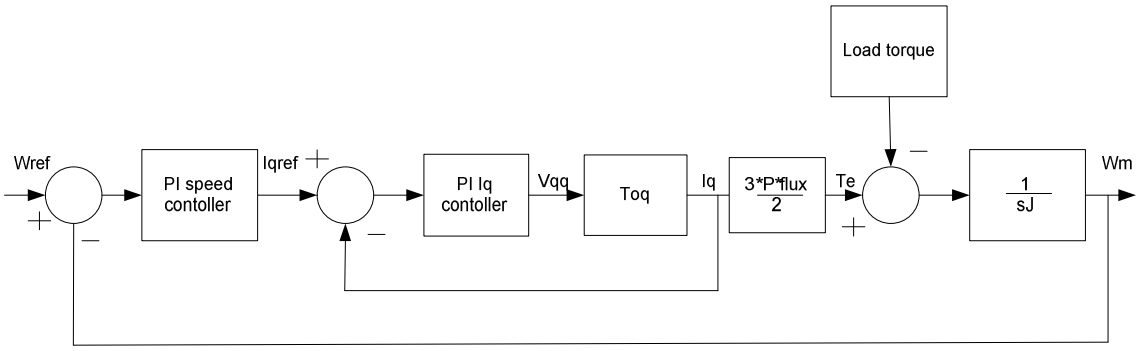

Figure 5.6: Speed control loop: PMSM Speed Control

where the PI speed controller is given by $C_2 = K_p + \frac{K_i}{s}$

$$T_{cw} = \frac{T_{ow}}{1 + T_{ow}} \tag{5.27}$$

The characteristic equation is given by

$$a(s) = 1 + T_{ow} \tag{5.28}$$

Substituting T_{ow}, we get,

$$a(s) = Js^4 + 290Js^3 + (250J + 150P\lambda_m K_p)s^2 + 1.5P\lambda_m 100(K_p + K_i)s + 150P\lambda_m K_i \tag{5.29}$$

Substituting the motor parameters, we get,

$$a(s) = 9.6e-4s^4 + 0.2784s^3 + (0.24 + 22.77K_p)s^2 + 22.77(K_p + K_i)s + 22.77K_i \tag{5.30}$$

Applying the Rouths stability criterion , we get, $k_i > 0$ and $6.603K_i + 2277(K_p)^2 + 1776K_pK_i + 2277K_p + 1776K_i > 0$.

The $K_i = 100$ and $K_p = 10$ values gave satisfactory results. The results of applying these gains are shown in Figure 5.7,5.8:

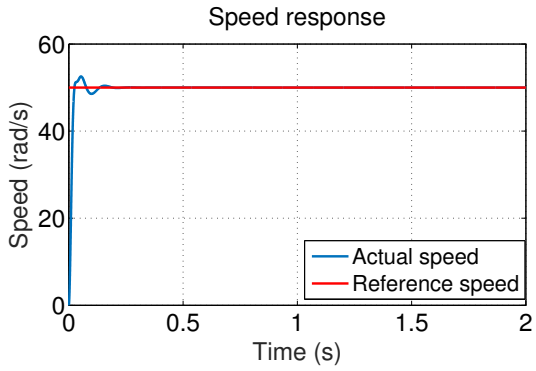

Figure 5.7: PMSM Simulation Speed Response: 0 to 50 rad/s

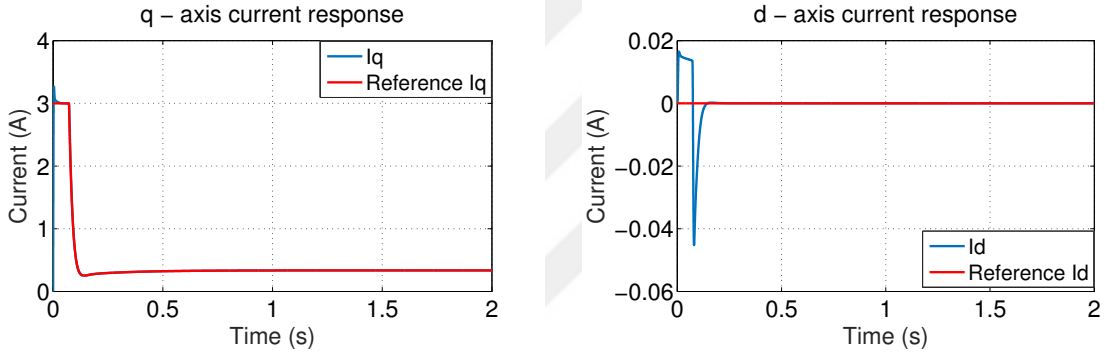

(a) PMSM Quadrature axis current response

(b) PMSM Direct axis current response

Figure 5.8: PMSM Speed Reference: 0 to 50 rad/s

It can be seen in Figure 5.7,5.8 that the speed and dq axis currents follow their references in steady state. However, there is about 4% overshoot in the speed response. One of the possible reasons for this overshoot could be the unavailability of the exact motor parameters and unmodelled dynamics. The motor parameters were estimated using the hardware experiments but may be inaccurate due to a limitation of the current sensor used in the experiment.

5.2.2 IM Control system design

The inner control loop for the flux and torque is designed using equation 3.91-3.95. They are as follows:

$$\frac{di_d}{dt} = -\gamma i_d + \eta\beta\lambda_d + w_e i_q + \frac{u_d}{\sigma L_s} \tag{5.31}$$

$$\frac{di_q}{dt} = -\gamma i_q - w_e\beta\gamma_d - w_e i_d + \frac{u_q}{\sigma L_s} \tag{5.32}$$

$$\frac{d\lambda_d}{dt} = -\eta\gamma_d + \eta L_h i_d \tag{5.33}$$

$$T_e = 1.5P\frac{L_h}{L_r}\lambda_d i_q \tag{5.34}$$

In order to control the flux and the torque, we need them in terms of the input variables u_d and u_q. To get that, we differentiate equation 5.33 and 5.34 with respect to time,

$$\frac{d^2\lambda_d}{dt^2} = -\eta\frac{d\lambda_d}{dt} + \eta L_h\frac{d\lambda_d}{dt} \tag{5.35}$$

Substituting i_d from equation 5.31 we get

$$\frac{d^2\lambda_d}{dt^2} = -\eta\frac{d\lambda_d}{dt} + \eta L_h(-\eta i_d + \eta\beta\lambda_d + w_e i_q + \frac{u_d}{\sigma L_s}) \tag{5.36}$$

$$\frac{d^2\lambda_d}{dt^2} = -\eta\frac{d\lambda_d}{dt} + \eta^2 L_h\beta\lambda_d + u_{dd} \tag{5.37}$$

Where, $u_{dd} = \eta L_h(-\gamma i_d w_e i_q + \frac{u_d}{\sigma L_s})$

Taking Laplace transform

$$s^2\lambda_d = -\eta\lambda_d s + \eta^2 L_h\beta\lambda_d + u_{dd} \tag{5.38}$$

$$\frac{\lambda_d}{u_{dd}} = \frac{1}{s^2 + \eta s - \eta^2 L_h\beta} = T_{of} \tag{5.39}$$

Applying PI controller to this loop, the closed loop transfer function can be written as

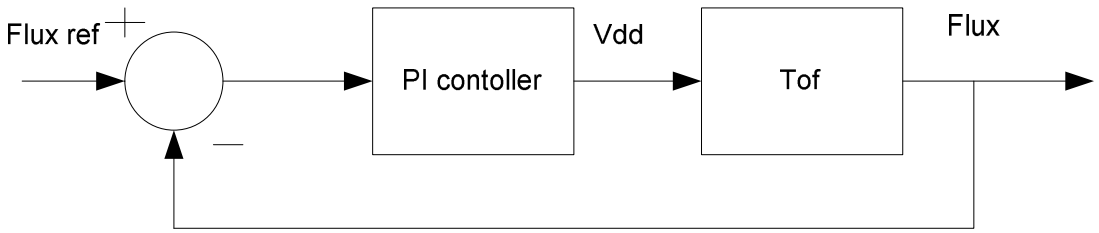

Figure 5.9: Flux control loop: IM Speed Control

$$T_{cf} = \frac{C_1 T_{of}}{1 + C_1 T_{of}} \tag{5.40}$$

Where, $C_1 = K_p + \frac{K_i}{s}$ is the PI controller for the flux.

The characteristic equation for the above transfer function is

$$a(s) = 1 + C_1 T_{of} \tag{5.41}$$

Substituting the C_1 and T_{of}, we get,

$$a(s) = s^3 + \eta s^2 + (K_p - \eta^2 L_h \beta)s + K_i \tag{5.42}$$

Substituting the motor parameters,

$$a(s) = s^3 + 8.58s^2 + (K_p - 3122)s + K_i \tag{5.43}$$

The Rouths Stability criterion gives us $Ki > 0$ and $K_p > 3122 + K_i/8.5$

The simulation works satisfactorily for K_p= 4000 and K_i=100

Similarly for the torque loop, the relation between the torque and the input u_q can be found by differentiating the torque equation

$$T_e = 1.5P\frac{L_h}{L_r}\lambda_d i_q \tag{5.44}$$

Since the flux is dependent on the speed and is constant for a speed, its derivative with respect to time is zero. Therefore,

$$\frac{dT_e}{dt} = 1.5P\frac{L_h}{L_r}\lambda_d \frac{di_q}{dt} \tag{5.45}$$

$$\frac{dT_e}{dt} = 1.5P\frac{L_h}{L_r}\lambda_d(-\gamma i_q - w_e\beta\lambda_d - w_e i_d + \frac{u_q}{\sigma L_s}) \tag{5.46}$$

$$\frac{dT_e}{dt} = 1.5P\frac{L_h}{L_r}\lambda_d i_q + 1.5P\frac{L_h}{L_r}\lambda_d u_{qq} \tag{5.47}$$

Where, $u_{qq} = -w_e\beta\lambda_d - w_e i_d + \frac{u_q}{\sigma L_s}$

$$\frac{dT_e}{dt} = -\gamma T_e + C u_{qq} \tag{5.48}$$

Where, $C = 1.5P\frac{L_h}{L_r}\lambda_d$

Taking laplace transform,

$$sT_e = -\gamma T_e + C u_{qq} \tag{5.49}$$

$$\frac{T_e}{u_{qq}} = \frac{C}{s+\gamma} = T_{ot} \tag{5.50}$$

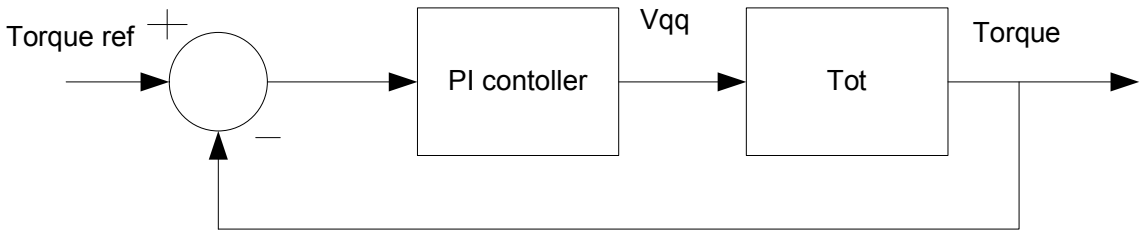

Figure 5.10: Torque control loop: IM Speed Control

The closed loop transfer function is given by,

$$T_{ct} = \frac{C_2 T_{ot}}{1 + C_2 T_{ot}} \tag{5.51}$$

Where, $C_2 = K_p + \frac{K_i}{s}$ is the PI controller for torque

The characteristic equation for the above transfer function is

$$a(s) = 1 + C_2 T_{ot} \tag{5.52}$$

Substitutint C_2 and T_{ot}

$$a(s) = s^2 + (K_p C + \gamma)s + K_i C \tag{5.53}$$

Substituting the motor parameters, we get,

$$a(s) = s^2 + (0.122K_p + 48.4)s + 0.122K_i \tag{5.54}$$

Appying the Rouths Stability criterion, $K_i > 0$ and $K_p > -400$

The simulation works satisfactorily for $K_p = 100$ and $K_i = 1000$

The outer speed control loop is as shown in Figure 5.11.

$$T_{ow} = \frac{C_3 T_{ct} 1.5P}{sJ} \tag{5.55}$$

Where, $C_3 = K_p + \frac{K_i}{s}$ is the speed PI controller

The closed loop transfer function can be written as

$$T_{cw} = \frac{T_{ow}}{1 + T_{ow}} \tag{5.56}$$

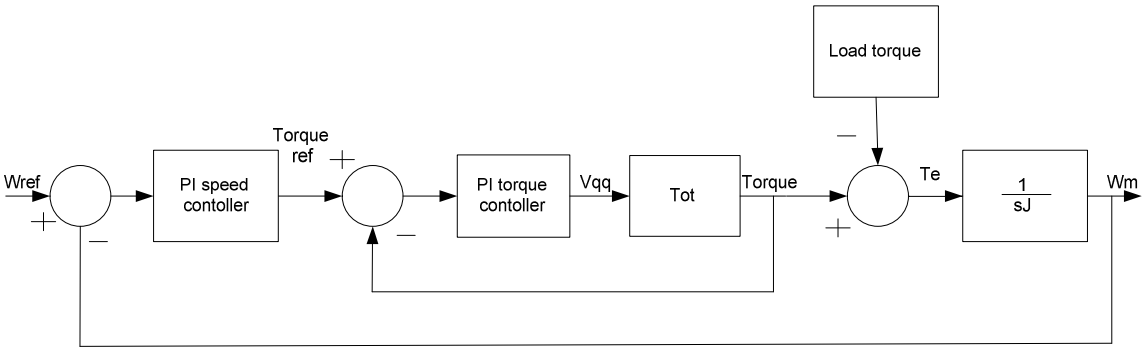

Figure 5.11: Speed control loop: IM Speed Control

The characteristic equation for the above transfer function is

$$a(s) = 1 + T_{ow} \tag{5.57}$$

Substituting T_{ow}, we get,

$$a(s) = s^3(1 + K_pCJ) + s^2(\gamma + 100C + 1000CK_pJ + 100CK_iJ) + s(1000K_iCJ + 1000) \tag{5.58}$$

Substituting the motor parameters, we get,

$$a(s) = s^3(1 + 1.17e - 4K_p) + s^2(170 + 0.11K_p + 0.011K_i) + s(0.11K_i + 1000) \tag{5.59}$$

Applying the Rouths Stability criterion we get, $0.11K_i + 1000 > 0$ And $170 + 0.11K_p + 0.11K_i > 0$

The simulation works satisfactorily for $K_p = 0.1$ and $K_i = 5$

The results of these simulations are shown in Figure 5.12-5.13

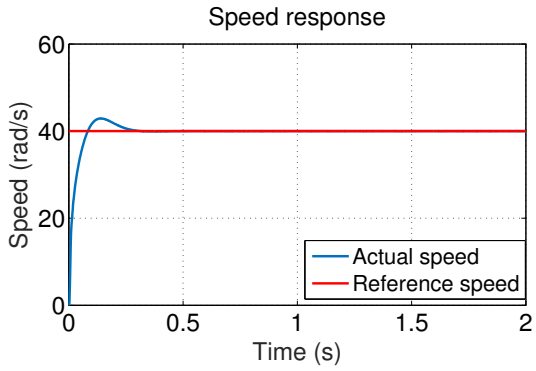

Figure 5.12: IM Simulation Speed Response:0 rad/s to 40 rad/s

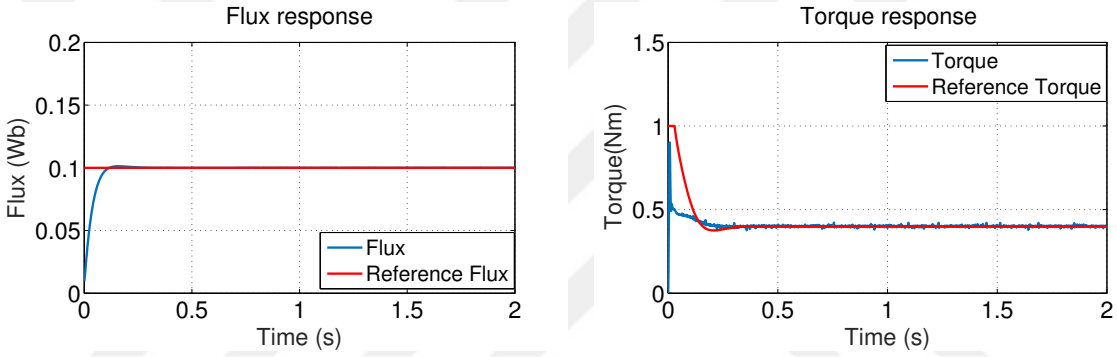

(a) Flux response

(b) Torque response

Figure 5.13: IM Simulation Speed reference: 0 to 40 rad/s

It can be seen in Figure 5.12-5.13 that the speed, flux and torque follow their references in steady state. The flux and torque are following their references within 0.2 seconds. In the speed response, there is about 7% overshoot. This overshoot is similar to the one found in the PMSM simulation could also be due to the unavailability of motor parameters and unmodelled dynamics.

Chapter 6

Experimental results

The setup is used to perform speed control algorithms on DC and AC motors. The connections and procedure to perform these experiments are discussed in the following sections along with experimental results.

6.1 DC motor

The speed control experiment on a Permanent magnet DC motor is implemented in this section.

6.1.1 Components

The components that will be used in this experiment are PMDC Stator, DC 60V and 18V Power supplies, Microcontroller, Power converter board, DB9 connecting cables.

6.1.2 Connections

1. Connect a power supply to the DC bus voltage point and set it to 60V, 3A maximum current. Set the second power supply to 5V and connect it to the current sensor power supply point on the board.

2. Connect the power converter board to the micro-controller and the rotor terminals using the two DB9 cables.

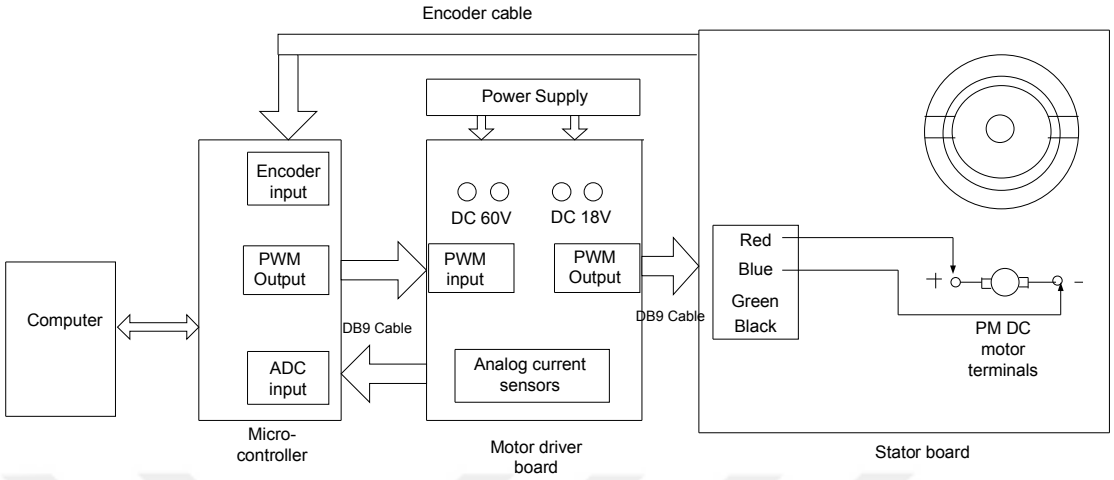

Figure 6.1: Setup connections for DC motor speed control experiment

3. The cable from the converter board has 4 connections points, of which only two will be required. Connect the red cable to the positive terminal on the motor housing board and the blue cable to the negative terminal.

4. Connect the encoder cable coming from the motor to the eQEP module pins of the micro-controller.

5. Now, connect the micro-controller to the PC and turn the switch on the controller to ON position.

6.1.3 Procedure

1. Launch MATLAB and 'Run' the main.m file.

2. Click on the DC motor push button to open the DC motor user interface.

3. Set the reference speed at the top of the window by entering a signed 5 digit number. Incase the number is two or one digit, enter 0's before the number to make it 5 digit. For example, if you want to set the reference speed to 3 rad/s, enter: +00003 in the specified box. Similarly for a reference of -30 rad/s, enter: -00030.

4. Click on the 'Start' push button to start the motor operation and observer the speed and current waveforms.

5. The PID controller gains are changed by entering values in the respective boxes. Enter a signed 5 digit value in the boxes next to the name of the controller gain. Similar to the case of reference speed, if the value has less than 5 digits, add zeros at the beginning to make a total 5 digits.

6. The effect of change of the PID controller gains can be seen in the speed and current response.

7. Enter different reference speed and observer the speed and current response.

6.1.4 Results

To support the simulated results, the same experiments are performed using the setup described in the previous chapter. The tuning of PI controllers is done by trial and error method. In this method the integral gain, K_i is set to zero. Then, the proportional gain, K_p is increased until the output is close to the set reference value. If there is a steady state error, the integral gain K_i is increased from zero till the error is removed.

1st reference speed: A step reference of 0 to 30 rad/s is given to the motor. Its current and speed responses are as shown in Figure 6.2.

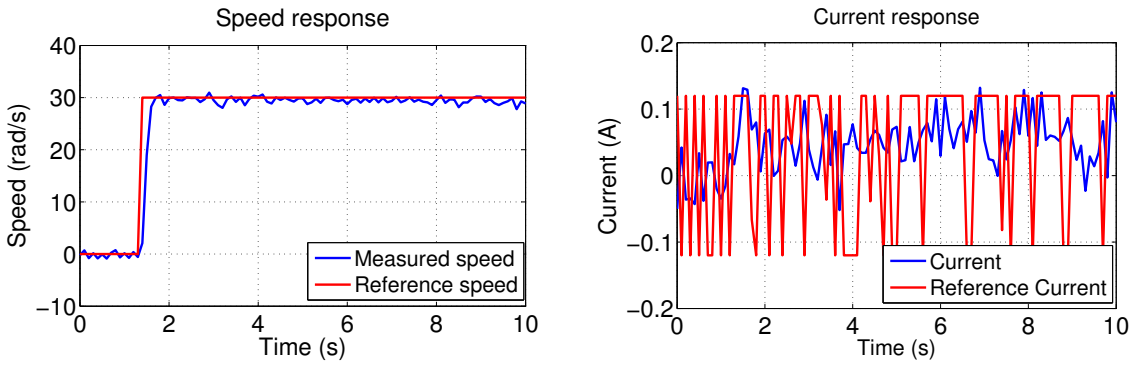

(a) Speed Response

(b) Current Response

Figure 6.2: DC Motor Experimental positive Speed reference : 0 to 30 rad/s

It can be seen that the steady state motor speed is nearly the same as the reference speed. However, if the motor current goes below 20mA then the motor speed does not follow the reference speed accurately. The reason for this behavior is the limitation in the resolution of the current sensor. Since the sensor we used has a resolution of 20mA, it was unable to detect the motor current below 20mA resulting in addition of noise in the current measurement, thereby effecting the control action and the causing the speed to deviate from the reference.

2nd reference speed: A step reference of 0 to -30 rad/s is given to the motor. Its current and speed responses are as shown in Figure 6.3.

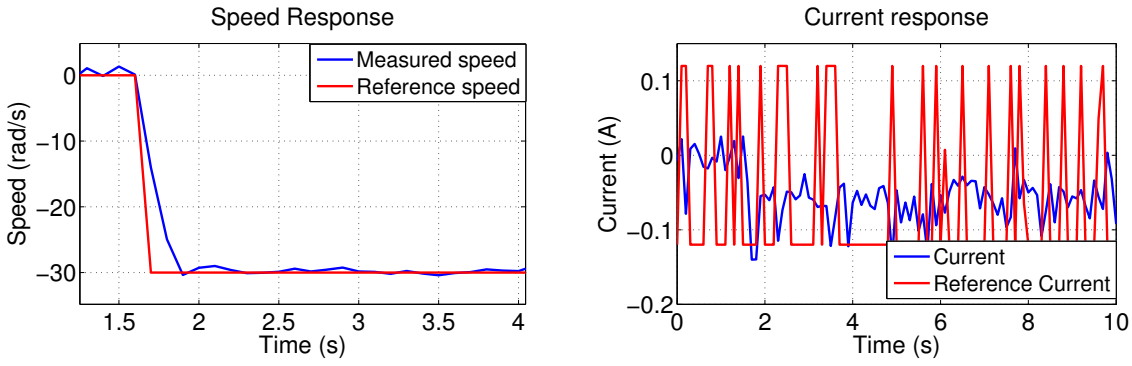

(a) Speed Response

(b) Current Response

Figure 6.3: DC Motor Experimental negative Speed reference : 0 to -30 rad/s

The transient and steady state response is similar to the type 1 reference speed response. This shows that the controller is working for both positive and negative references.

6.2 PMSM speed control

The speed control experiment on PMSM is implemented in this section.

6.2.1 Components

The components that will be used in this experiment are AC Stator,2/4 pole permanent magnet rotor, DC 60V and 18V Power supplies, Microcontroller, Power converter board, DB9 connecting cables.

6.2.2 Connections

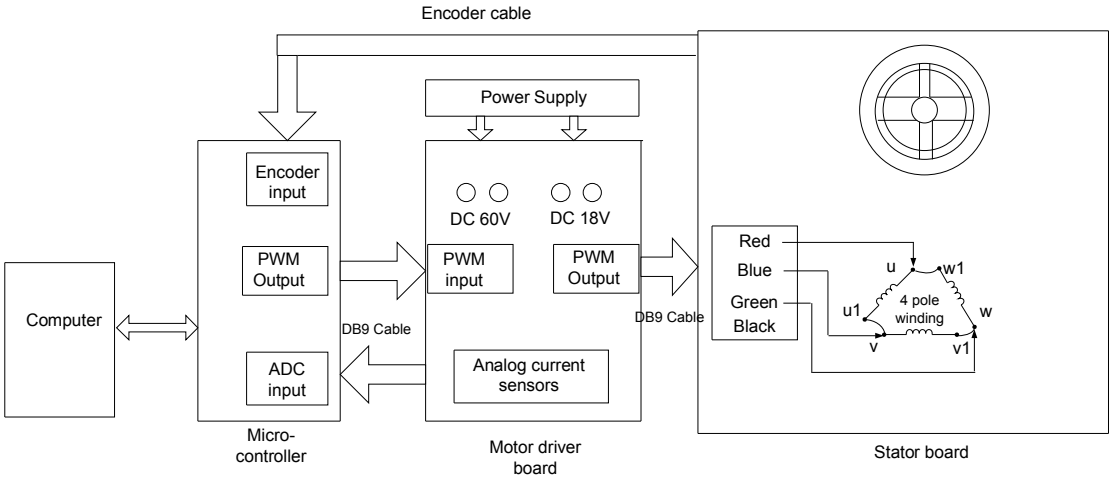

Figure 6.4: Setup connections for PMSM speed control experiment

1. The power supply connections are the same as done in the DC motor experiment.
2. The difference is in the cable connections between the motor driver board and the stator board.

3. The red, blue and green cables represent the three phase input to the stator and are connected to the U, V and W points in the stator board.

4. The AC stator can be used with multiple rotors. Unscrew the stator bracket and insert the 2/4 pole permanent magnet rotor in the stator. Close the bracket and ensure the rotor is connected properly by rotating it by hand.

5. The stator can be made up of either 4 or 8 poles connected in a star or a delta fashion.

6. A star connection of the 4 pole stator is shown in Figure 6.4.

7. Connect the micro-controller to the PC and turn it on.

6.2.3 Procedure

1. Launch MATLAB and 'Run' the main.m file.

2. Click on the PM synchronous motor push button to open its user interface.

3. Set the reference speed at the top of the window by entering a signed 5 digit number. Similar to the case of DC motor, if the reference speed has one or two digits, add zeros to make it a 5 digit number.

4. The rotor flux of the PMSM needs to be aligned with the d-axis to accurately perform the Clark-Park transformation. This is done using the 'Align' text box. When the 'Align' value is +1, the rotor is positioned in a way to align the rotor flux with the d-axis. By default the 'Align' value is set to +1.

5. Click on 'Start' push button and enter +00002 in the 'Align' text box to start to start the motor operation after flux alignment with d-axis.

6. The motor speed and the dq axis currents can also be observed in the interface.

7. The effect of change of the PID controller gains of the three PI loops can be seen by editing its value. Similar to the case of DC motor, enter a signed 5 digit

value in the boxes next to the controller gains and observe the speed and current response.

8. Enter different reference speeds and observer the speed and current response.

6.2.4 Results

1st reference speed: A step reference of 0 to 50 rad/s is given to the motor at t=0 sec. Its current and speed responses are as shown in Figure 6.5-6.6.

The steady state motor speed is same as that of the reference. The d-axis current is

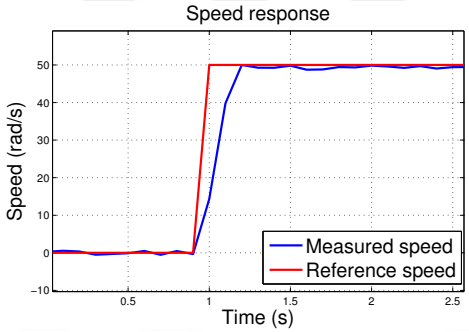

Figure 6.5: PMSM Experimental Speed Response: 0 to 50 rad/s

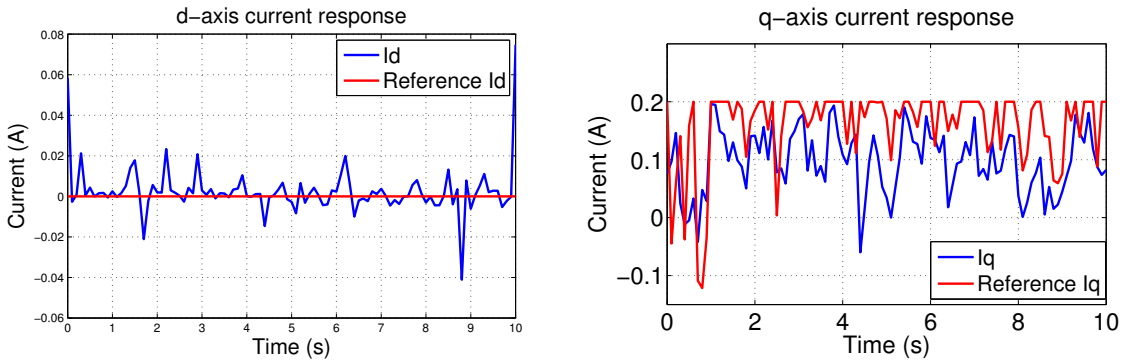

(a) Direct axis current response

(b) Quadrature axis current response

Figure 6.6: PMSM Experimental positive Speed reference: 0 to 50 rad/s

within 8-14mA range for a reference of 0mA. The q-axis current is also following its reference although with a small steady state error of 10-15 mA.

2nd reference speed: A step reference of 0 to -50 rad/s is given to the motor at t=0 sec.

Its current and speed responses are as shown in Figure 6.7-6.8.

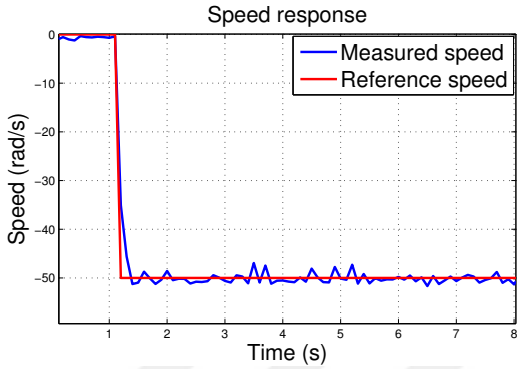

Figure 6.7: PMSM Experimental Speed Response: 0 to -50 rad/s

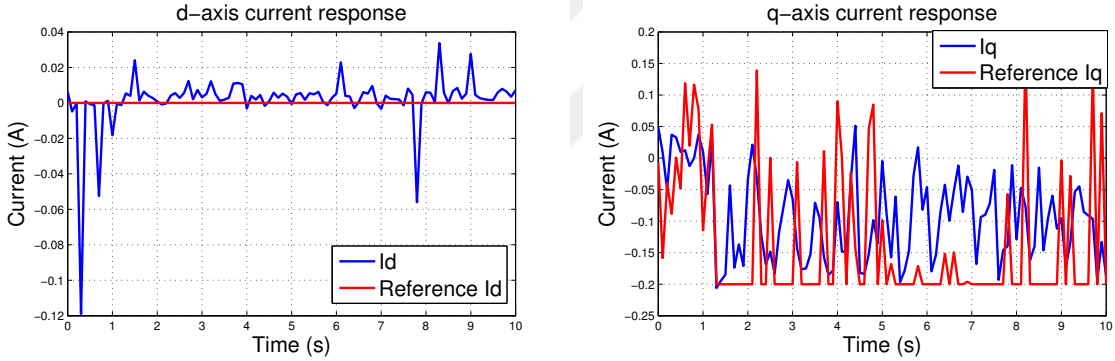

(a) Direct axis current response

(b) Quadrature axis current response

Figure 6.8: PMSM Experimental negative Speed reference: 0 to -50 rad/s

Similar to the 1st reference input, the steady state motor speed is same as that of the reference. The speed of the motor deviates from the reference if the current is near or below 20mA. The d-axis current is within 5-10mA range for a reference of 0mA. The q-axis current is also following its reference although with a small steady state error of 25 mA. This shows that the controller performance is same for both positive and negative references.

6.3 IM speed control

The speed control experiment on induction motor is implemented in this section.

6.3.1 Components

The components that will be used in this experiment are AC Stator,Squirrel cage copper/ brass rotor, DC 60V and 18V Power supplies, Microcontroller, Power converter board, DB9 connecting cables.

6.3.2 Connections

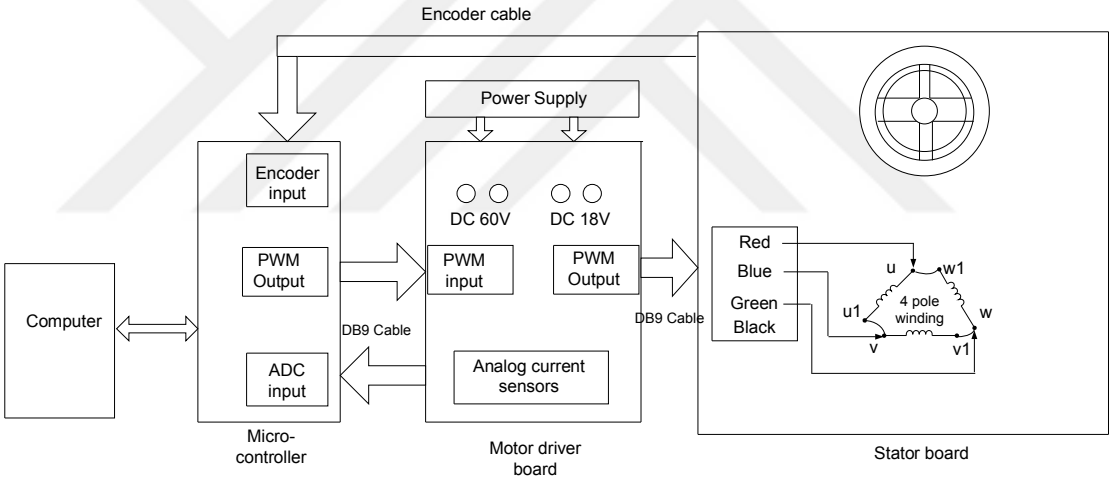

Figure 6.9: Setup connections of IM speed controller experiment

1. The connections are exactly same as that for the PMSM but with only difference of the rotor.

2. Connect the brass/copper squirrel cage rotor in the AC stator. After placing it inside ensure that the rotor is connected properly by giving it a spin.

3. Similar to the PMSM, the AC stator can be made up of either 4 or 8 poles and connected in a star or a delta fashion.

4. A star connection of the 4 pole stator is shown in Figure 6.9.

5. Connect the micro-controller to the PC and turn it on.

6.3.3 Procedure

1. The experiment procedure is similar to the PMSM with the difference of the rotor alignment. In case of IM, the motor does not need to be aligned with the d-axis.

2. Launch MATLAB and 'Run' the main.m file.

3. Click on the induction motor push button to open its user interface.

4. Set the reference speed at the top of the window by entering a signed 5 digit number. Similar to the case of DC motor, add zeros to make it a 5 digit number.

5. The motor speed and the dq axis currents can also be observed in the user interface.

6. The effect of change of the PID controller gains of the three PI loops can be seen by editing its value. Similar to the case of DC motor, enter a signed 5 digit value in the boxes next to the controller gains and observe the speed and current response.

7. Enter different reference speeds and observer the speed and current response.

6.3.4 Results

1st reference speed: A step reference of 0 to 40 rad/s is given to the motor. Its flux, torque and speed responses are as shown in Figure 6.10-6.11.

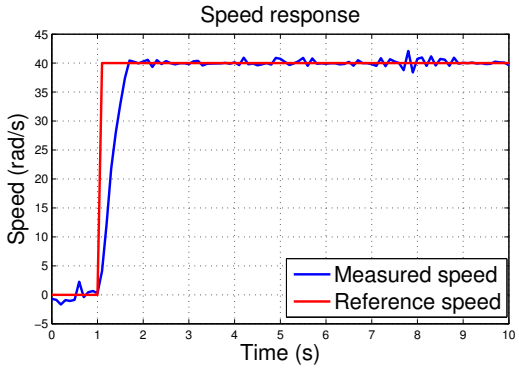

Figure 6.10: IM Experimental Speed Response:0 rad/s to 40 rad/s

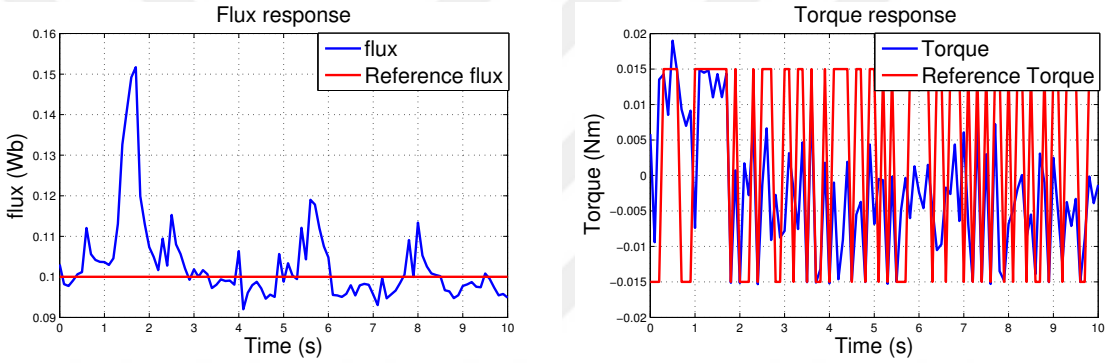

(a) Flux response

(b) Torque response

Figure 6.11: IM Experimental positive Speed reference: 0 to 40 rad/s

The steady state motor speed is same as that of the reference. Similar to the experimental results of DC motor and PMSM, the deviation of the motor speed from the reference is due to the lowering of the current consumption below 20mA. The flux and torque responses are also following their respective references.

2nd reference speed: A step reference of 0 to -40 rad/s is given to the motor. Its current and speed responses are as shown in Figure 6.12-6.13.

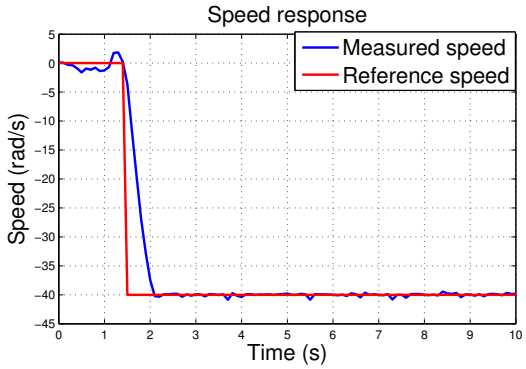

Figure 6.12: IM Experimental Speed Response:0 rad/s to -40 rad/s

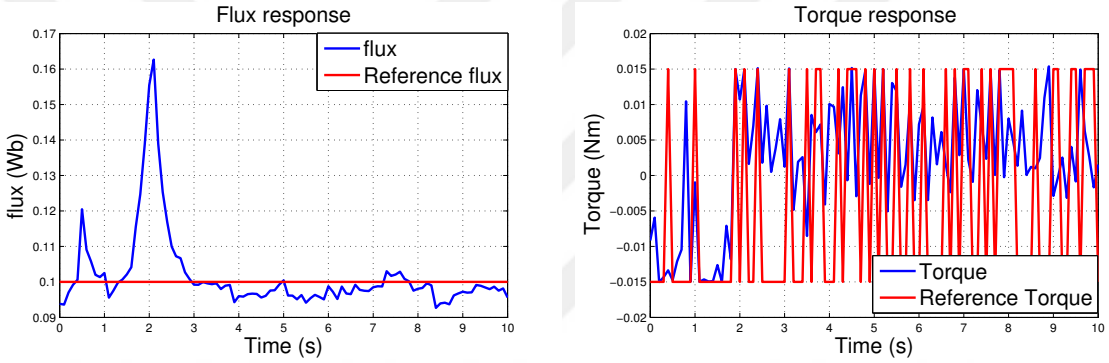

(a) Flux response

(b) Torque response

Figure 6.13: IM Experimental negative Speed reference: 0 to -40 rad/s

It can be seen that the steady state speed and torque responses are similar to the 1st reference with the difference of the opposite sign. This shows that the controller is working for both the positive and negative speed references. The flux is maintained at the same value hence has the same response as 1st reference input.

Chapter 7

Conclusion

In this thesis, a compact laboratory setup has been built to act as a teaching aid for understanding the basics as well as control techniques of electrical machines. It is capable of implementing speed control techniques on electrical machines. Field Oriented Control and cascaded PI controllers were used for implementing the speed control of AC and DC motors respectively. A power converter board driven from a low cost and fast digital signal processor is also added. A GUI is also developed for easy interaction with the DSP. This setup can be used for performing advanced control techniques like Sliding mode control, Optimal control, Fuzzy logic and Neural network based controllers. Advanced switching techniques like Space Vector PWM can also be used to generate the 3-phase AC signal. The future work of this thesis can include the application of control techniques to other machines such as Stepper motor. It can also include extending this setup to include a web based remote laboratory.

Appendix A

Micro-controller programming

The steps involved in programming the controller using CCS is as follows: Launch CCS version 5 or later. The main window of the CCS is as shown in Fig A.1

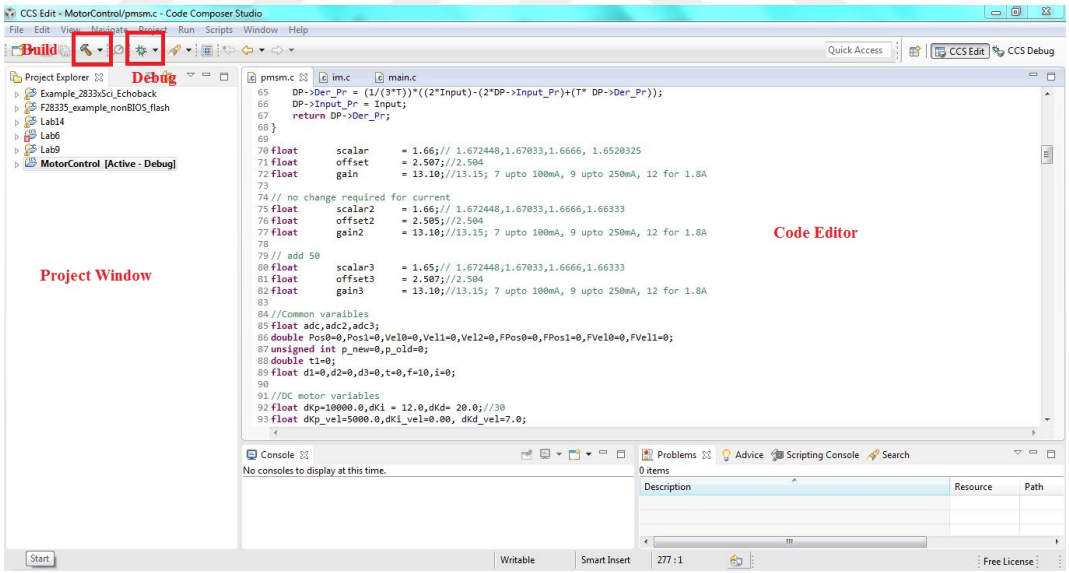

Figure A.1: Code composer studio: Window in Edit mode

This window is the edit mode of the CCS, where we can edit code and build projects. The coding is done in the editor window and is built and checked for errors using the build icon. The project explorer/window allows us to access multiple projects, which are activated by clicking on the project name. The code is downloaded into the controller using the Debug icon.

To create a new project

1. Click on File-New-CCS project

2. Enter Target-2833x and select TMS320F28335 from the adjoining drop down list. Enter a project name (MotorControl) and click on Finish.

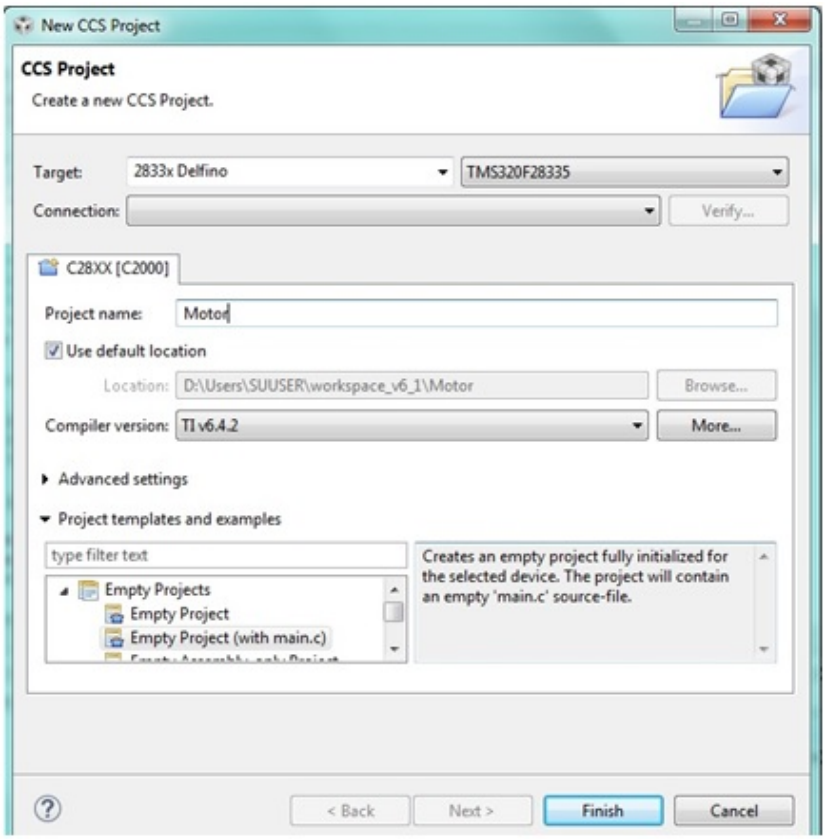

Figure A.2: Creating a new project

3. Define the size of the C system stack. In the project window, right click at project "MotorControl" and select "Properties". In category "C/C++ Build", "C2000 Linker", "Basic Options" set the C stack size to 0x400.

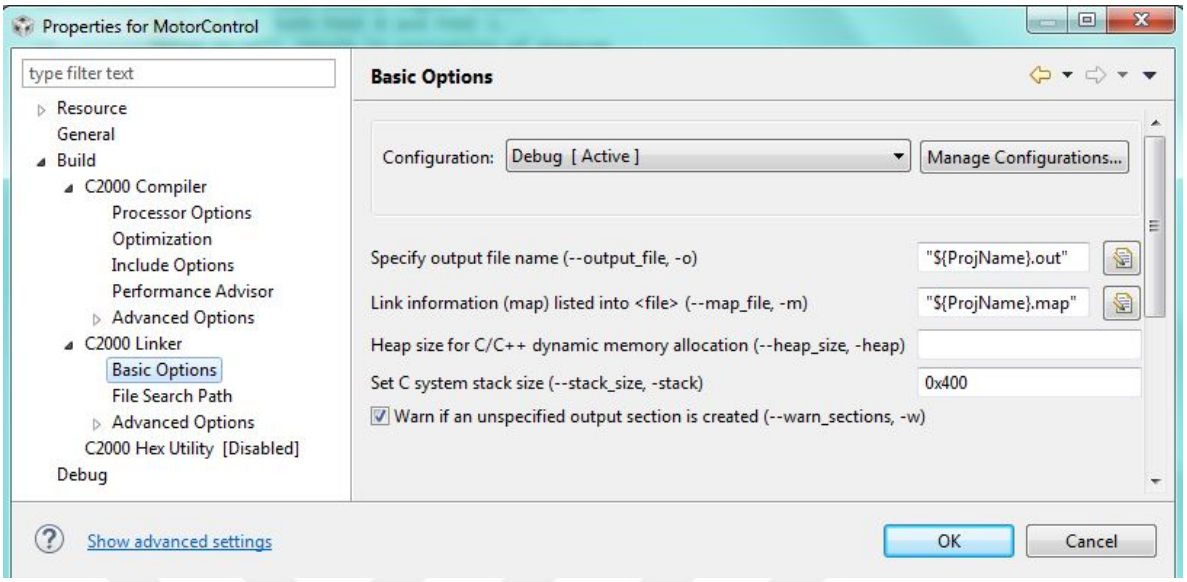

Figure A.3: Size of the C system stack

4. Now, write the C code for the motor in the main.c file

   Next, we need to add some initialization files which have been provided by TI

5. In the C/C++ perspective, right click at project "MotorControl" and select "Link Files to Project".

   Go to folder

   ‘‘C:\tidcs\c28\dsp2833x\v131\DSP2833x_headers\source’’ and link:

   DSP2833x_GlobalVariableDefs.c

   This file defines all global variable names to access memory mapped peripheral registers.

6. Repeat the "Link Files to Project" step. From

   C:\tidcs\c28\dsp2833x\v131\DSP2833x_common\source add:

   DSP2833x_CodeStartBranch.asm

   DSP2833x_SysCtrl.c

   DSP2833x_ADC_cal.asm

   DSP2833x_usDelay.asm

```
DSP2833x_Adc.c
DSP2833x_CpuTimers.c
DSP2833x_DefaultIsr.c
DSP2833x_Eqep.c
DSP2833x_GlobalVariableDefs.c
DSP2833x_PieCtrl.c
DSP2833x_PieVect.c
```

7. From

```
C:\tidcs\c28\dsp2833x\v131\DSP2833x_headers\cmd link to project
"MotorControl":
DSP2833x_Headers_nonBIOS.cmd
```

This linker command file will connect all global register variables to their corresponding physical addresses.

We also have to extend the search path of the C-Compiler for include files. Right click at project "MotorControl" and select "Properties". Select "C/C++ Build", "C2000 Compiler", "Include Options".

In the box "Add dir to include search path", add the following lines:

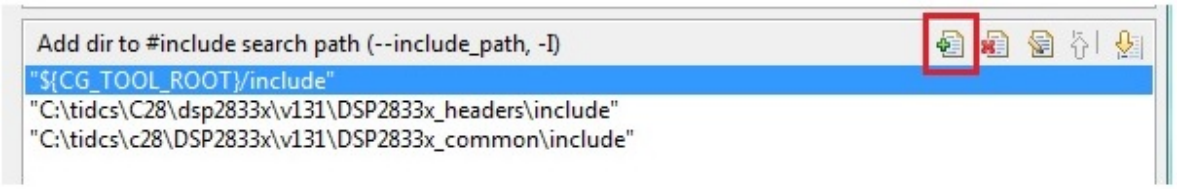

Figure A.4: Add additional paths to include header and common files

```
C:\tidcs\C28\dsp2833x\v131\DSP2833x_headers\include
C:\tidcs\c28\DSP2833x\v131\DSP2833x_common\include
```

The code is loaded into the device using the debug icon, indicated in Figure A.1. When the debugger is launched the CCS switches to the debug mode from the edit mode. The

window appearance has also changed with some additional features as shown in Figure A.5.

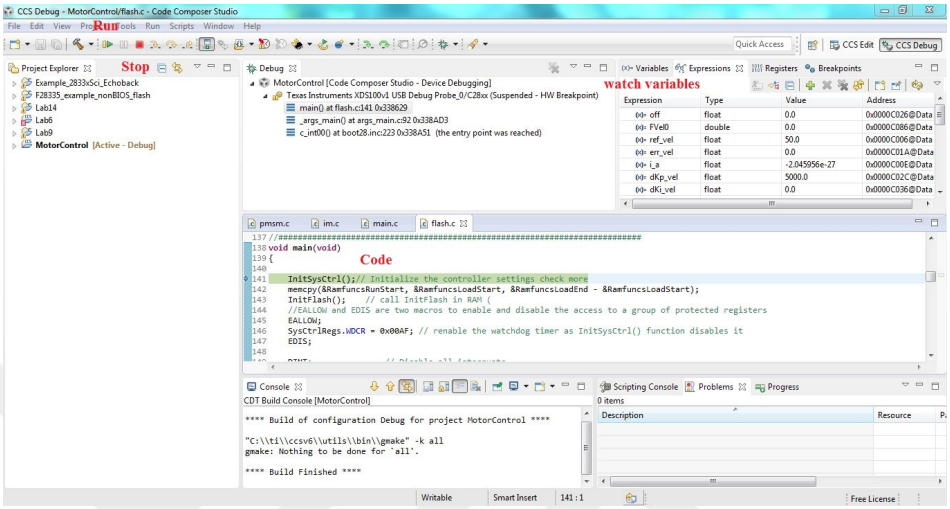

Figure A.5: Code composer studio: Window in Run mode

The watch window is used to observe the variable values and to modify those values if need be. The gains of the PID controller can be changed and its effect on the speed and current values can be seen in this window.

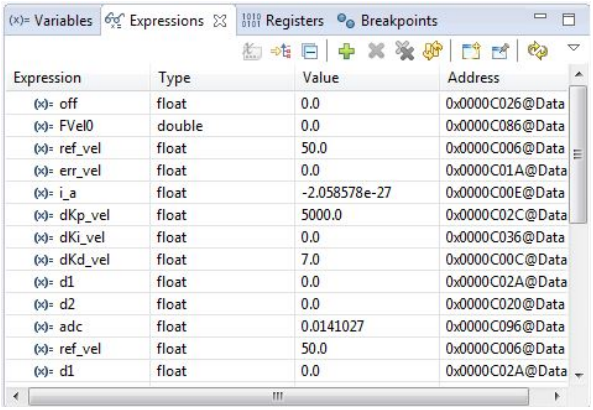

Expression	Type	Value	Address
(x)= off	float	0.0	0x0000C026@Data
(x)= FVel0	double	0.0	0x0000C086@Data
(x)= ref_vel	float	50.0	0x0000C006@Data
(x)= err_vel	float	0.0	0x0000C01A@Data
(x)= i_a	float	-2.058578e-27	0x0000C00E@Data
(x)= dKp_vel	float	5000.0	0x0000C02C@Data
(x)= dKi_vel	float	0.0	0x0000C036@Data
(x)= dKd_vel	float	7.0	0x0000C00C@Data
(x)= d1	float	0.0	0x0000C02A@Data
(x)= d2	float	0.0	0x0000C020@Data
(x)= adc	float	0.0141027	0x0000C096@Data
(x)= ref_vel	float	50.0	0x0000C006@Data
(x)= d1	float	0.0	0x0000C02A@Data

Figure A.6: CCS variable watch window

All the variables used in the code can be added in the watch window. A new variable can be added by clicking on the '+' icon next to the 'Add new expression'. The experiments on the DC and AC machines can be performed by simply writing the code in the main.c file.

Appendix B

Simulink models

DC motor model is implemented in Simulink as follows

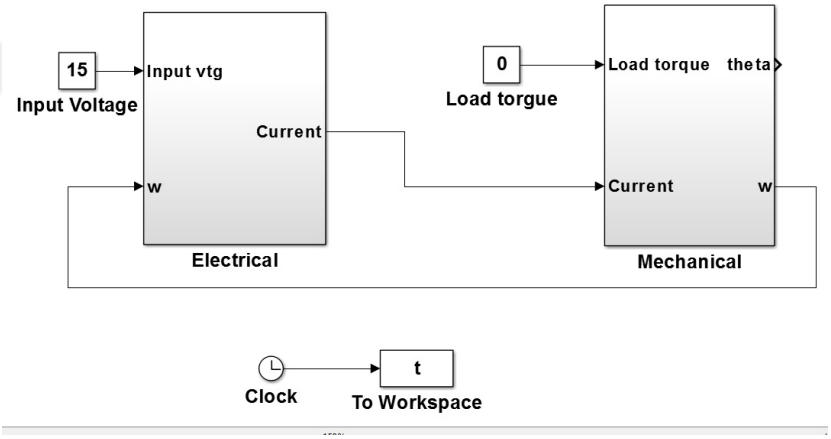

Figure B.1: DC motor Simulink model

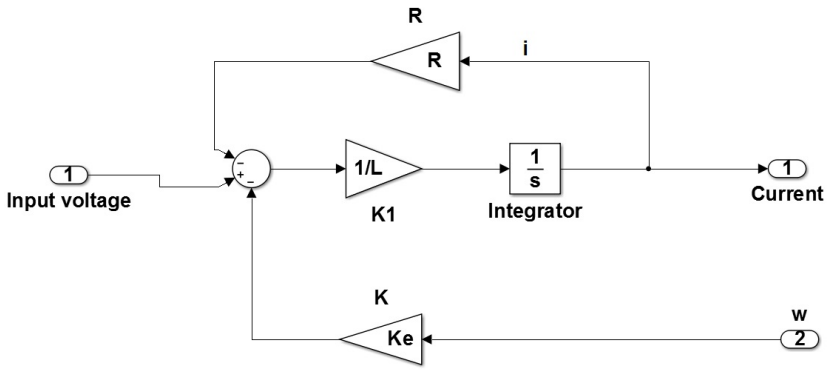

Figure B.2: DC motor Simulink model: electrical module

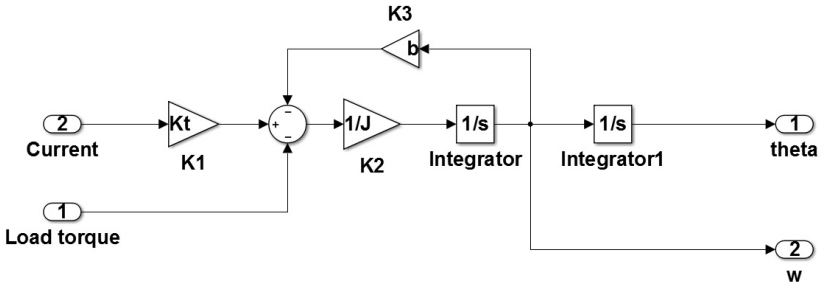

Figure B.3: DC motor Simulink model: mechanical module

The DC motor paramters are as follows:

```
R = 11.8; L = 0.028; b= 2.4152e-05; J=6*b; Kt = 0.318; Ke= 0.318;
```

PMSM Simulink model

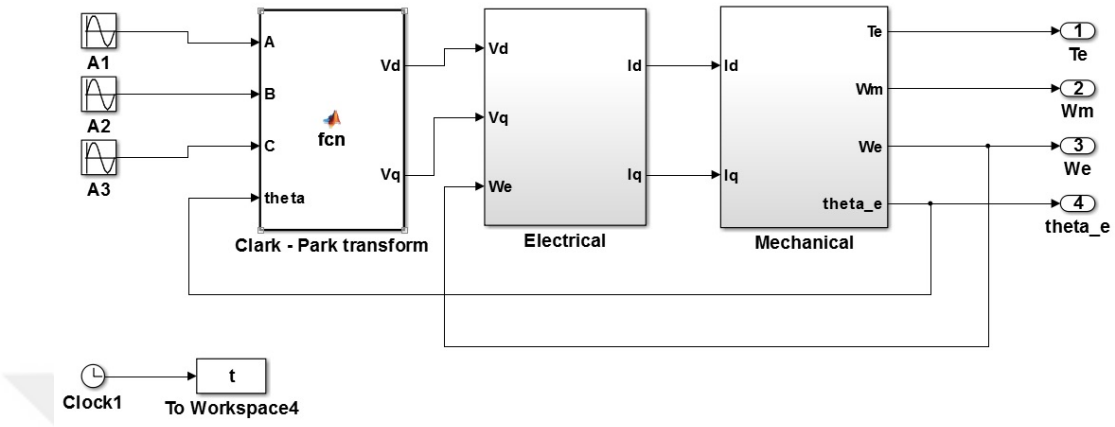

Figure B.4: PMSM Simulink model

The Clark-Park transformation function is as follows:

```
function [Vd, Vq] = fcn(A,B,C, theta)
Val=A;
Vbt=0.577*(A+2*B);
Vd = Val*cos(theta)+Vbt*sin(theta);
Vq =  -Val*sin(theta)+Vbt*cos(theta);
```

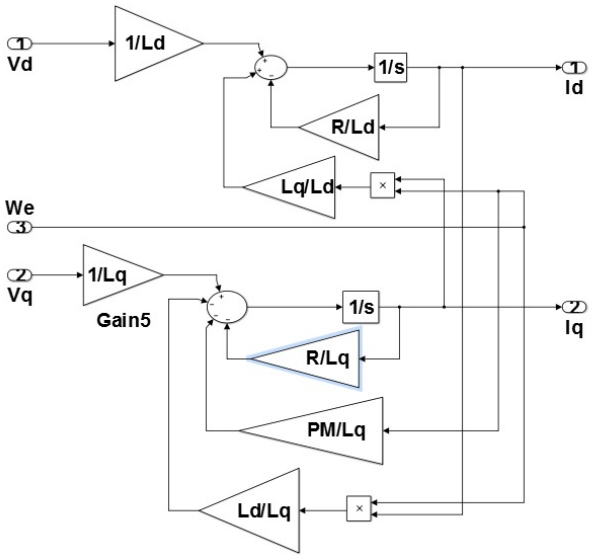

Figure B.5: PMSM Simulink model: Electrical module

Electrical module

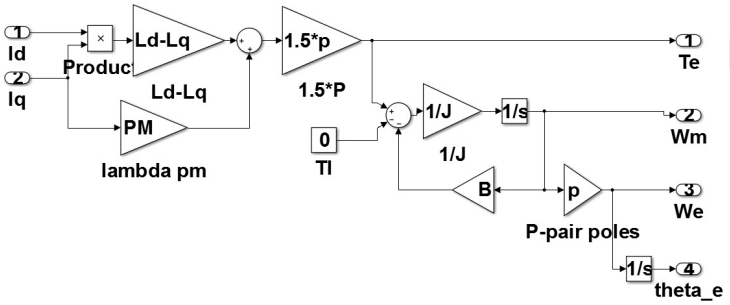

Figure B.6: PMSM Simulink model: Mechanical module

Mechanical module

The PMSM paramters are as follows:

```
Ld= 0.4; Lq= 0.4; R=16; PM=0.0759; K= 0.00153;J= 0.0009645;
```

IM Simulink model

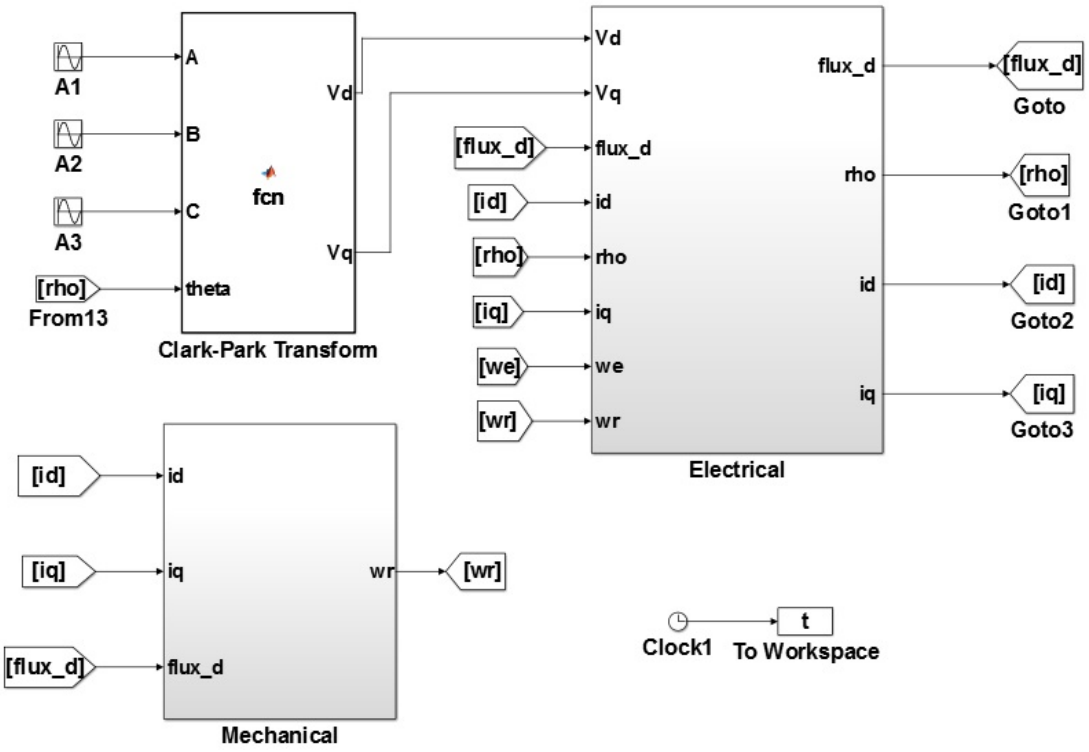

Figure B.7: IM Simulink model

The Clark-Park transformation function is as follows:

```
function [Vd, Vq] = fcn(A,B,C, theta)
Val=A;
Vbt=0.577*(A+2*B);
Vd = Val*cos(theta)+Vbt*sin(theta);
Vq =  -Val*sin(theta)+Vbt*cos(theta);
```

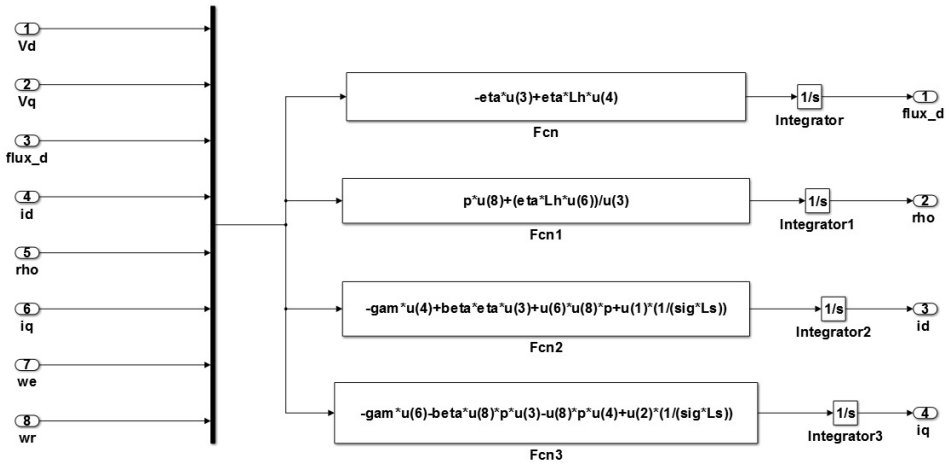

Figure B.8: IM Simulink model: electrical module

The electrical sub-system consists of the equations of I_d, I_q, flux and position of the rotor flux. The mechanical sub-system consists of the equations of the torque and electrical motion.

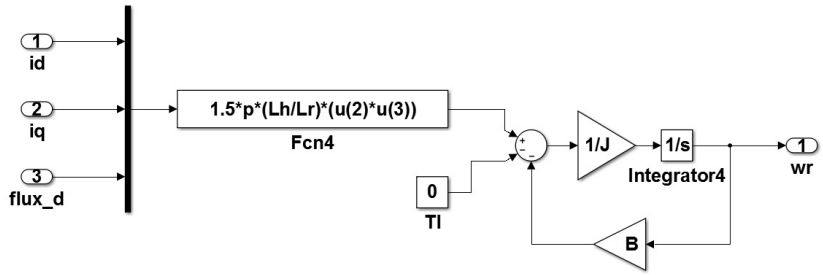

Figure B.9: IM Simulink model: mechanical module

The IM paramters are as follows:

```
Rs=22; Rr=18.4; Lh=0.875; Ls=0.875; Lr=2.143; J=9.645e-4; B=1.5e-3; p=4;
```

Appendix C

Speed control flowcharts

DC Motor Speed control

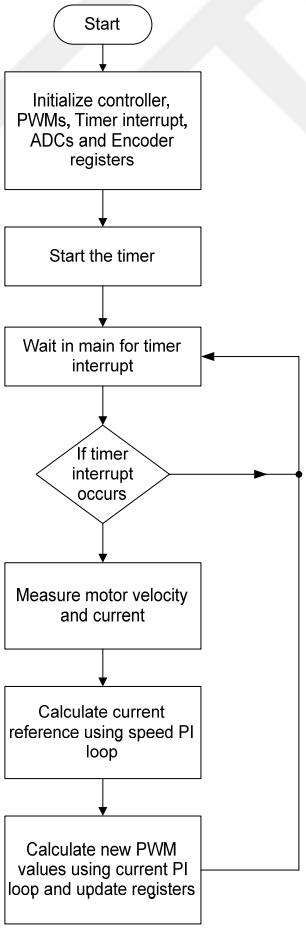

Figure C.1: DC motor Speed Control flowchart

AC motor speed control

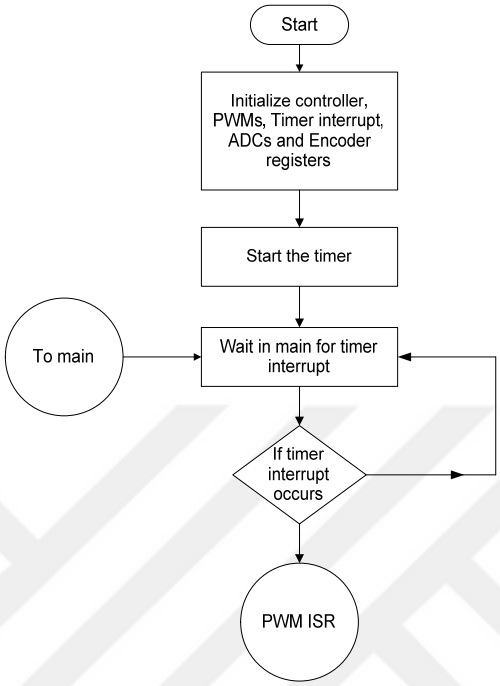

Figure C.2: AC motor Speed Control flowchart

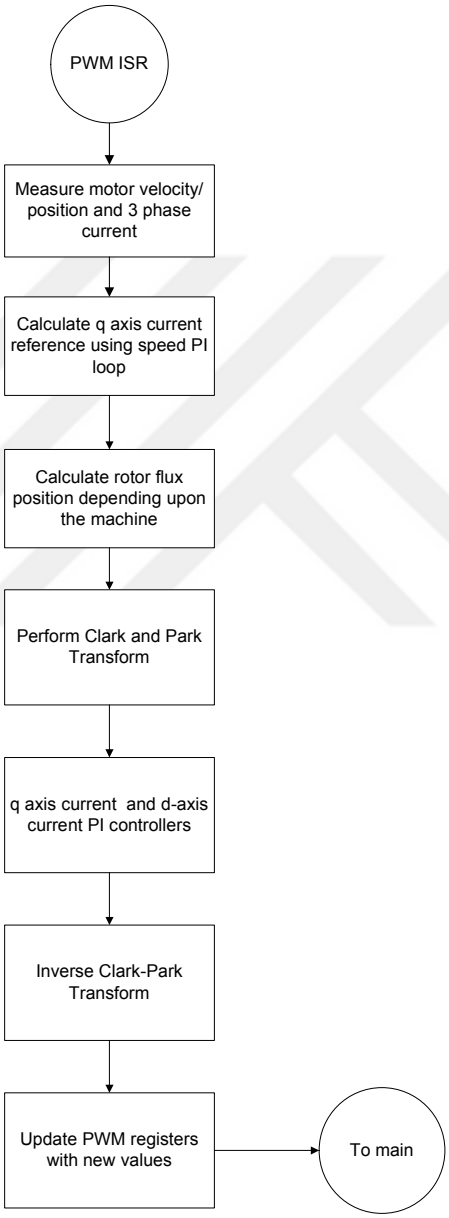

Figure C.3: AC motor Speed Control: Interrupt subroutine flowchart

Bibliography

[1] R. C. Panaitescu, N. Mohan, W. Robbins, P. Jose, T. Begalke, C. Henze, T. Undeland, and E. Persson, "An instructional laboratory for the revival of electric machines and drives courses," in *Power Electronics Specialists Conference, 2002. pesc 02. 2002 IEEE 33rd Annual*, vol. 2, pp. 455–460, IEEE, 2002.

[2] M. Y. Alsmadi, "New trends and technologies in power electronics and motor drives educa-tion," *age*, vol. 24, p. 1.

[3] W. Robbins, N. Mohan, P. Jose, T. Begalke, C. Henze, and T. Undeland, "A building-block-based power electronics instructional laboratory," in *Power Electronics Specialists Conference, 2002. pesc 02. 2002 IEEE 33rd Annual*, vol. 2, pp. 467–472, IEEE, 2002.

[4] N. Mohan, *Electric drives: an integrative approach*. 2003.

[5] P. T. Krein, "A broad-based laboratory for power electronics and electric machines," in *Power Electronics Specialists Conference, 1993. PESC'93 Record., 24th Annual IEEE*, pp. 959–964, IEEE, 1993.

[6] R. S. Balog, Z. Sorchini, J. W. Kimball, P. L. Chapman, and P. T. Krein, "Modern laboratory-based education for power electronics and electric machines," *IEEE Transactions on Power Systems*, vol. 20, no. 2, pp. 538–547, 2005.

[7] Z. Zhang, C. T. Hansen, and M. A. Andersen, "Teaching power electronics with a design-oriented, project-based learning method at the technical university of denmark," *IEEE Transactions on Education*, vol. 59, no. 1, pp. 32–38, 2016.

[8] B. J. Barron, D. L. Schwartz, N. J. Vye, A. Moore, A. Petrosino, L. Zech, and J. D. Bransford, "Doing with understanding: Lessons from research on problem- and project-based learning," *Journal of the Learning Sciences*, vol. 7, no. 3-4, pp. 271–311, 1998.

[9] P. C. Blumenfeld, E. Soloway, R. W. Marx, J. S. Krajcik, M. Guzdial, and A. Palincsar, "Motivating project-based learning: Sustaining the doing, supporting the learning," *Educational psychologist*, vol. 26, no. 3-4, pp. 369–398, 1991.

[10] R. H. Chu, D. D.-C. Lu, and S. Sathiakumar, "Project-based lab teaching for power electronics and drives," *IEEE transactions on education*, vol. 51, no. 1, pp. 108–113, 2008.

[11] L. Goel, T. Lie, A. Maswood, and G. Shrestha, "Enhancing power engineering education through the use of design modules," *IEEE transactions on power systems*, vol. 11, no. 3, pp. 1131–1138, 1996.

[12] C. Ferrater-Simon, L. Molas-Balada, O. Gomis-Bellmunt, N. Lorenzo-Martínez, O. Bayó-Puxan, and R. Villafafila-Robles, "A remote laboratory platform for electrical drive control using programmable logic controllers," *IEEE transactions on education*, vol. 52, no. 3, pp. 425–435, 2009.

[13] F. Blaabjerg, "A power electronics and drives curriculum with project-oriented and problem-based learning: A dynamic teaching approach for the future," *Journal of Power Electronics*, vol. 2, no. 4, pp. 240–249, 2002.

[14] C.-M. Ong, *Dynamic simulation of electric machinery: using MATLAB/SIMULINK*, vol. 5. Prentice Hall PTR Upper Saddle River, NJ, 1998.

[15] T. Zhao and Q. Wang, "Application of matlab/simulink and pspice simulation in teaching power electronics and electric drive system," in *2005 International Conference on Electrical Machines and Systems*, vol. 3, pp. 2037–2041, IEEE, 2005.

[16] Z. Raud, V. Vodovozov, T. Lehtla, and E. Pettai, "Simulation tools to study power electronics," in *Power Electronics and Applications, 2009. EPE'09. 13th European Conference on*, pp. 1–9, IEEE, 2009.

[17] S. Li and R. Challoo, "Restructuring an electric machinery course with an integrative approach and computer-assisted teaching methodology," *IEEE Transactions on Education*, vol. 49, no. 1, pp. 16–28, 2006.

[18] C. A. Canizares and Z. T. Faur, "Advantages and disadvantages of using various computer tools in electrical engineering courses," *IEEE Transactions on education*, vol. 40, no. 3, pp. 166–171, 1997.

[19] J. Ma and J. V. Nickerson, "Hands-on, simulated, and remote laboratories: A comparative literature review," *ACM Computing Surveys (CSUR)*, vol. 38, no. 3, p. 7, 2006.

[20] D. Magin and S. Kanapathipillai, "Engineering students' understanding of the role of experimentation," *European journal of engineering education*, vol. 25, no. 4, pp. 351–358, 2000.

[21] W. G. Hurley and C. K. Lee, "Development, implementation, and assessment of a web-based power electronics laboratory," *IEEE Transactions on Education*, vol. 48, no. 4, pp. 567–573, 2005.

[22] K. Yeung and J. Huang, "Development of a remote-access laboratory: a dc motor control experiment," *Computers in Industry*, vol. 52, no. 3, pp. 305–311, 2003.

[23] H. H. Hahn and M. W. Spong, "Remote laboratories for control education," in *Decision and Control, 2000. Proceedings of the 39th IEEE Conference on*, vol. 1, pp. 895–900, IEEE, 2000.

[24] V. Silva, V. Carvalho, R. Vasconcelos, and F. Soares, "Remote pid control of a dc motor," 2007.

[25] C. C. Ko, B. M. Chen, J. Chen, Y. Zhuang, and K. C. Tan, "Development of a web-based laboratory for control experiments on a coupled tank apparatus," *IEEE Transactions on education*, vol. 44, no. 1, pp. 76–86, 2001.

[26] M. Corradini, G. Ippoliti, T. Leo, and S. Longhi, "An internet based laboratory for control education," in *Decision and Control, 2001. Proceedings of the 40th IEEE Conference on*, vol. 3, pp. 2833–2838, IEEE, 2001.

[27] M. Basso and G. Bagni, "Artist: a real-time interactive simulink-based telelab," in *Computer Aided Control Systems Design, 2004 IEEE International Symposium on*, pp. 196–201, IEEE, 2004.

[28] J. Sánchez, S. Dormido, R. Pastor, and F. Morilla, "A java/matlab-based environment for remote control system laboratories: illustrated with an inverted pendulum," *IEEE Transactions on Education*, vol. 47, no. 3, pp. 321–329, 2004.

[29] M. H. Rashid, *Power electronics handbook: devices, circuits and applications*. Academic press, 2010.

[30] R. W. Erickson and D. Maksimovic, *Fundamentals of power electronics*. Springer Science & Business Media, 2007.

[31] N. Mohan and T. M. Undeland, *Power electronics: converters, applications, and design*. John Wiley & Sons, 2007.

[32] V. I. Utkin and A. Sabanovic, "Sliding modes applications in power electronics and motion control systems," in *Industrial Electronics, 1999. ISIE'99. Proceedings of the IEEE International Symposium on*, vol. 1, pp. TU22–TU31, IEEE, 1999.

[33] A. Sabanovic, L. M. Fridman, and S. K. Spurgeon, *Variable structure systems: from principles to implementation*, vol. 66. IET, 2004.

[34] A. Sabanović and N. Sabanović-Behlilović, "Sliding modes in electrical drives and motion control," *IFAC Proceedings Volumes*, vol. 44, no. 1, pp. 756–761, 2011.

[35] A. Sabanovic and F. Bilalovic, "Sliding mode control of ac drives," *IEEE Transactions on Industry Applications*, vol. 25, no. 1, pp. 70–75, 1989.

[36] N. Sabanovic-Behlilovic, A. Sabanovic, and T. Ninomiya, "Pwm in three-phase switching converters-sliding mode solution," in *Power Electronics Specialists Conference, PESC'94 Record., 25th Annual IEEE*, pp. 560–565, IEEE, 1994.

[37] A. Šabanović, K. Jezernik, and N. Šabanović, "Sliding modes applications in power electronics and electrical drives," in *Variable structure systems: towards the 21st Century*, pp. 223–251, Springer, 2002.

[38] N. S. Nise, "Control system engineering, 4\(ˆ{th}\) edition," 2003.

[39] K. Ogata, *Modern control engineering*. Prentice Hall PTR, 2001.

[40] F. Harashima and S. Kondo, "A design method for digital speed control system of motor drives," in *Power Electronics Specialists conference, 1982 IEEE*, pp. 289–297, IEEE, 1982.

[41] E. Yolacan, S. Aydin, H. M. Ertunc, *et al.*, "Real time dsp based pid and state feedback control of a brushed dc motor.," in *ICAT*, pp. 1–6, 2011.

[42] J. J. Gude, E. Kahoraho, and J. Etxaniz, "Practical aspects of pid controllers: An industrial experience," in *Emerging Technologies and Factory Automation, 2006. ETFA'06. IEEE Conference on*, pp. 870–878, IEEE, 2006.

[43] F. Blaschke, "The principle of field orientation as applied to the new transvektor closed-loop control system for rotating field machines," 1972.

[44] L. Jisha and A. Thomas, "A comparative study on scalar and vector control of induction motor drives," in *Circuits, Controls and Communications (CCUBE), 2013 International conference on*, pp. 1–5, IEEE, 2013.

[45] M. Bhardwaj, "Sensored field oriented control of 3-phase permanent magnet synchronous motors," *Texas Instruments, Inc*, 2013.

[46] B. Akin and M. Bhardwaj, "Sensored field oriented control of 3-phase induction motors," *Texas Instruments Incorporated*, 2013.